· U C ·

FCTUC FACULDADE DE CIÊNCIAS
E TECNOLOGIA
UNIVERSIDADE DE COIMBRA

DEPARTAMENTO DE
ENGENHARIA MECÂNICA

Electrical and Tribological Properties of DLC Coatings

Submitted in Partial Fulfillment of the Requirements for the Degree of Master in Materials Engineering

Author

Matej Janež

Supervisors

Bruno Trindade, PhD

Mitjan Kalin, PhD

Jury

President	**Professor Albano Cavaleiro, PhD** **University of Coimbra**
Vowel	**Professor Anne Neville, PhD** **University of Leeds**
Advisor	**Professor Mitjan Kalin, PhD** **University of Ljubljana**

In the framework of Joint European Master in Tribology of Surfaces and Interfaces

tribos joint european master in tribology of surfaces and interfaces
Ljubljana • Leeds • Coimbra • Luleå

Coimbra, July 2015

University of Coimbra
Faculty of Science and Technology
Department of Mechanical Engineering
Erasmus Mundus TRIBOS

Electrical and Tribological Properties of DLC Coatings

Author: Matej Janež
Supervisors: Professor Mitjan Kalin, PhD
Professor Bruno Trindade, PhD

Coimbra, July 2015

Resumo

Os revestimentos DLC têm atraído o interesse da comunidade científica devido à sua combinação única de propriedades. São geralmente usados em várias aplicações sob a forma de revestimentos protetores uma vez que apresentam baixo atrito e elavada resistência ao desgaste. No entanto, existem poucas referências na literatura sobre valores de propriedades elétricas de revestimentos DLC e as suas potencialidades em aplicações eléctricas. O foco deste trabalho incidiu na determinação e análise das propriedades elétricas e tribológicas de revestimentos DLC comerciais.

Neste trabalho foram estudados a resistividade, o atrito e a resistência ao desgaste de quatro revestimentos de DLC e de diferentes aços à temperatura por deslizamento alternativo a seco e diferentes condições de corrente continua.

Os revestimentos DLC estudados neste trabalho foram Ti-DLC (5 e 10 % at.Ti) e W-DLC (5 e 10 % at.W). Os testes realizados permitiram medir o coeficiente atrito e, simultaneamente, a resistividade no contacto, usando um tribómetro pino-disco e um equipamento de medição de tensão. A microscopia óptica e a interferometria de luz branca foram utilizads para a análise das pistas de desgaste. Os resultados das medições de resistividade mostraram que todos os revestimentos eram contudores eléctricos. Observou-se ainda que concentrações mais elevadas do elemento dopante conduziam a uma menor resistividade no contato. O contacto DLC – DLC também produziu medições de condutividade superior em comparação com o contacto DLC – aço. Os valores da resistividade estática são substancialmente inferiores aos obtidos por resistividade deslizante, confirmando-se assim que o deslizamento tem um grande efeito sobre a condutividade de contato. Tal como esperado, os valores do coeficientes de atrito obtidos para os pares DLC – aço e DLC – DLC são inferiors aos obtidos para o contato aço – aço. O par W-DLC – W-DLC com 10 % at. W foi o que apresentou maior potencial para aplicações elétricas, com muito baixos valores de resistividade elétrica e coeficiente de atrito e baixa taxa de desgaste.

Os resultados obtidos neste trabalho indicam que os revestimentos DLC têm propriedades eléctricas promisoras, sendo potenciais materiais para futuras aplicações elétricas.

Abstract

DLC coatings have attracted interest of many researches due to their unique combination of properties. They are often used in various applications as protective coatings because of their excellent low friction and high wear resistance. However, little research has been done on the electric properties of DLC coatings and their possibilities in electric applications. The focus of this work was the analysis and comparison of electrical and tribological properties of selected commercial coatings in sliding electric contacts.

In the thesis, the resistance, friction and wear behavior of four different coatings, which were selected based on their good electrical and tribological properties observed during preliminary testing, were evaluated and compared to steel at room temperature in dry reciprocating sliding mode and under different direct current conditions. Commercial DLC coatings selected for the analysis were Low Ti-DLC (5 at.%), High Ti-DLC (10 at. %), Low W-DLC (5 at.%) and High W-DLC (10 at.%). The tests were performed by simultaneously gathering friction and resistance data in the contact using a ball-on-disc tribometer and a voltage drop measuring setup. Optical microscopy and white light interferometry were used for the analysis of the wear scars.

The results of the resistance measurements showed that all coatings conducted direct current. It was observed that higher doping element concentrations led to lower resistance of the contact. DLC – DLC contact also produced higher conductivity measurements compared to DLC – Steel contact. The conductivity of Steel – Steel contact was in a similar range as DLC – DLC contact. Static resistance was substantially lower than sliding resistance which confirms that sliding has a great effect on the conductivity of the contact. As expected, friction results displayed substantially lower friction coefficients for DLC – Steel and DLC – DLC contacts in comparison to Steel – Steel contact. The best material combination for electric application was High W-DLC – High W-DLC which exhibited very low electric resistance and friction coefficient with very low wear rate.

The results gathered in this work indicate that DLC coatings have promising electric properties and show potential in future electric applications.

Acknowledgments

First I would like to express my appreciation and gratitude to my supervisors, Dr. Mitjan Kalin and Dr. Bruno Trindade for their support and guidance during the course of this work. I would also like to thank Dr. Anne Neville and Dr. Albano Cavaleiro for their participation on the examination committee.

Sincere gratitude goes to Dr. Rok Simič for his assistance during this endeavor. I would like to thank him for his answers to my numerous questions regarding my thesis, the advice and assistance he has given me throughout my research and his inspiring instructions in the development and completion of this thesis.

I would also like to extend my gratitude to the whole staff of Laboratory for Tribology and Interface Nanotechnology in Ljubljana, particularly to Kosta Simonović, Blaž Žugelj, Dr. Janez Kogovšek, Joži Sterle and Franci Kopač, for their invaluable help and support during my research.

Thank you to the consortium of the TRIBOS master course, for giving me the opportunity to participate in the program. This international experience enabled me to broaden my horizons and further deepen my academic knowledge.

In the end, my deepest gratitude and appreciation goes to God, for giving me the strength and all of my talents, to my fiancée Maruša for her patience, love and constant encouragement and to my family, father Tomaž, mother Valerija, sister Kristina and brothers Tadej and Jernej for their unfailing support and patience throughout my studies.

Table of Contents

List of Figures

List of Tables

Symbols and Acronyms

Acronyms

AC – Alternating current

COF – Coefficient of friction

DC – Direct current

DLC – Diamond-like carbon

ECR-CVD – Electron cyclotron resonance chemical vapor deposition

FCA – Filtered cathodic arc deposition

IBD – Direct ion beam deposition

Me-DLC – Metal doped diamond-like carbon

PECVD – Plasma-enhanced chemical vapor deposition

RF – Radio frequency

Ti-DLC – Titanium doped diamond-like carbon

W-DLC – Wolfram doped diamond-like carbon

Symbols

100Cr6 – Steel grade

a-C – Non-hydrogenated amorphous carbon

a-C:H – Hydrogenated amorphous carbon

a-C:N – Nitrogenated amorphous carbon

at.% – Atomic percent

CH_2 – Methylene

C_2H_2 – Acetylene

C=N – Imine

C≡N – Nitrile

NH_2 – Amino group

Ra – Roughness parameter (arithmetic average of the absolute values)

sp^2 – Hybridized state

sp^3 – Hybridized state

ta-C – Tetrahedral amorphous carbon

TiC – Titanium carbide

1. Introduction

The synthesis of new coatings for tribological applications is a matter of great technological interest. Carbon exists in various forms and is used in numerous applications. It has been the topic of research of many scientists [1].

Diamond-like carbon (DLC) films are amorphous carbon films with a mixture of sp^2 and sp^3 hybrid bonding [2]. Diamond has high hardness, high friction coefficient, high thermal conductivity, low wear rates, wide band gap, chemical inertness and optical transparency. On the contrary, graphite is a well-known solid lubricant with its soft structure, has good electrical conductivity, low coefficient of friction but high wear rate. This combination of properties of DLC coatings proves them to be useful in many applications such as cutting and grinding tools, heat exchangers, infrared windows and high frequency high power electronic devices [3].

DLC can be grown as thin films on different substrates and captures desirable properties of both diamond and graphite such as low coefficient of friction and high wear resistance. Diamond-like carbon coatings can be produced by numerous different methods such as ion beam, DC or RF sputtering, cathodic arc deposition, pulsed laser deposition (PLD), and plasma enhanced chemical vapor deposition (PECVD). Depending on the deposition method used, the properties of the coatings can vary substantially [4, 5].

DLC is commonly doped with other elements that induce a change in material properties. Hydrogen is the most commonly used dopant in DLC films, with films generally being classified as hydrogenated or non hydrogenated. Other dopants used to modify the properties of DLC include nitrogen, oxygen, wolfram, titanium, boron, chromium, copper, platinum, silver, fluorine, and silicon. Post processing techniques such as surface treatments and annealing can further modify the properties of DLC films. Plasma treatments with oxygen, nitrogen, hydrogen, and carbon tetrafluoride can change contact angles. Laser and thermal annealing can reduce residual stresses [6, 7].

DLC protective coatings have already found numerous possible applications in many different industries including aerospace, automotive, auto racing, cosmetics, medical/dental implants and instruments, metal working, bearings, electronics, industrial wear parts, infrared optics, military, tools/dies/molds and textiles [8].

1.1 Scope and Motivation

Modern mechanical systems are expected to operate in increasingly more demanding conditions therefore the materials used have to constantly provide better and more diverse properties for the system to be more efficient and durable. Longer service life, ability to tolerate greater loads, ease and low cost of maintenance, environmental gain in conservation of resources, improved response in kinetic systems, lower energy consumption, resistance to corrosion, low friction, use of low cost base material, etc. are just a few good reasons for coating the machine parts of a mechanical systems.

Diamond-like carbon coatings are amorphous carbon coatings with well known low-friction and low-wear properties. They are being increasingly used in various systems because of their wear prevention properties and minimization of energy losses. However, many modern applications require good tribological performance along with efficient electrical conductivity. Examples of such systems are electrical motors, electrical switches, generators etc. Electrical contacts are in general not lubricated and this is where DLC coatings could provide a real benefit to such contacts, because of their excellent tribological properties without the presence of lubricants. Currently there is not a lot known on electrical properties of DLC coatings and how would DLC coatings behave in sliding contacts in relation to their electrical conductivity. There is still research needed to be done in order to determine which DLC coatings have the optimal electrical and tribological properties.

In this master thesis, the study of Diamond-like carbon films is conducted in relation to their electrical properties. The purpose of the work is to investigate the electrical properties of DLC films with the addition of different doping elements that could influence the electrical properties during tribological sliding. The study of tribological properties of DLC coatings was also done in order to observe the effects of electric current on friction and wear properties of DLC coatings and how electrical efficiency is influenced by different material combinations and electric current intensities in DLC contacts. The report of these effects would be of great importance and lead towards the improvements of electrical contact when using DLC coatings.

1.2 Goals of the Thesis

DLC films are suitable for a variety of applications due to their excellent mechanical properties, together with the possibility of tailoring the properties to specific requirements by varying the appropriate deposition conditions, film structure or doping them with different elements or compounds. DLC coatings are used in many modern industrial applications due to their excellent low friction and low wear properties but there is still a vast amount of research to be done to optimize the properties of DLC films for electronic applications.

The main objective of the thesis was to observe and compare the electrical properties of the commercially available DLC coatings doped with different elements and metals. It also studied the aforementioned characteristics effect on the friction and wear properties of the film, when voltage is applied. The aim of this research is to analyze the available DLC coatings and to determine which coatings show most promise for potential electrical applications.

The main points of this research were:

- comparative study of selected DLC films electrical and tribological properties
- study of tribological and electrical effects during DLC sliding under applied electrical conditions
- selection of the most promising coating among the selected commercial DLC coatings for electric conductivity applications

It is intended to develop an understanding of the electrical characteristics of the selected DLC coatings which would allow the optimization and design of a number of electrical applications. The research focused on the comparative study of the selected coatings and the reference material. Therefore it does not strive to produce the most electrically conductive DLC coating but rather provides an insight into performance and mechanisms of selected commercially available coatings.

1.3 Framework

The work presented was proposed by University of Ljubljana, which is one of the members of the consortium of the Joint European Master in Tribology of Surfaces and Interfaces – TRIBOS. The title of the thesis is Electrical and tribological properties of DLC films. The main objective of this work is to further explore new possibilities for DLC films in relation to their electrical properties and how the presence of an electric charge effects their tribological properties. In the scope and motivation section, the incentive for the research and the details of the issues are further explained. Main goals and aims of the research are presented in the subsequent section. The review of current literature and research on the subject is defined in the state of the art. Materials, testing equipment and procedures used in the research are described in the sections that follow. In the discussion and results section, the outcomes of the tests are presented and discussed. The final section contains a summary of what has been done and the conclusions that can be drawn from research. The referred literature used in the thesis is stated at the end.

2. State of the Art

2.1 Diamond-like Carbon Coatings

Solid materials, which are formed mainly of carbon, present excellent mechanical properties. Diamond exhibits very high hardness and thermal conductivity where on the other hand graphite has unusual softness and lubricity properties. Carbon is also the essential element in the synthesis of Diamond-like carbon coatings [9].

DLC coatings present maybe the largest and the most studied family among all coatings. They were first discovered by Schellenmeier in 1950 when he reported a black carbon film derived from C_2H_2 gas in glow-discharge plasma. His findings were not of much interest until 1980s and 1990s, when the research on DLC films gained momentum. Due to their excellent properties and performance characteristics, DLC coatings continue to draw a lot of attention from the scientific and industrial communities [1, 9].

The films are currently used in many industrial process where there is high demand for very good resistance to wear, scuffing, corrosion and erosion. Some examples of common DLC coating applications are presented in Figure 1. In the recent years, it has become easier to control the properties for the purpose of customizing them to meet the industrial application requirements for material durability and performance. Coatings made from DLC now represent one of the most interesting and important materials ever developed with numerous industrial applications. DLC is the only material that can at the same time provide high hardness and low friction in dry sliding conditions and the potential is almost endless. The films are used in various industrial applications such as microelectronics, optics, manufacturing, transportation, biomedical field, etc. and even found use in everyday devices, from razor blades to magnetic storage media. Over the last decades, there has been an increased development of new versions of DLC films, doped with different elements, including wolfram, titanium and chromium doped films. When combined with different duplex or multiplex surface treatments, DLC coatings can also provide additional functionality [8, 10, 11].

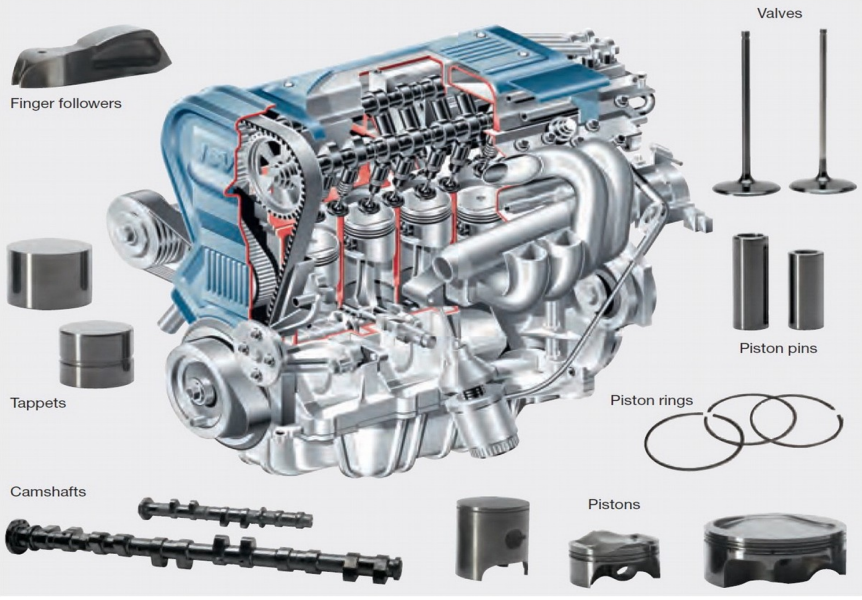

Figure 1: Selected engine parts coated with DLC [9]

Future applications of DLC coatings could also be found in sliding electric contacts, for instance in electric motors, generators and alternators. An example of such electric contact is shown in Figure 2. For some time now, the key materials for conducting current in sliding electric contacts are copper and graphite due to their combination of good electrical and tribological properties. To ensure proper current transfer and continuous contact between the components, the brushes must be pressed against the sliding contact with a sufficient load. This however promotes frictional losses and high wear rate of graphite brushes. Electrically conductive DLC coatings, together with their excellent low friction and high wear resistance properties, could pose as an excellent alternative to the current materials in use for electric contacts [12].

The present level of application of DLC films still does not reflect its true potential. In the near future, large-scale and low-cost manufacturing will definitely lead to wider application of DLC films. The need to further lower the cost, improve process reliability, reduce sensitivity to unexpected changes, production of high-quality coatings on different substrates are still required for the deposition of DLC films in large-volume applications [9, 13].

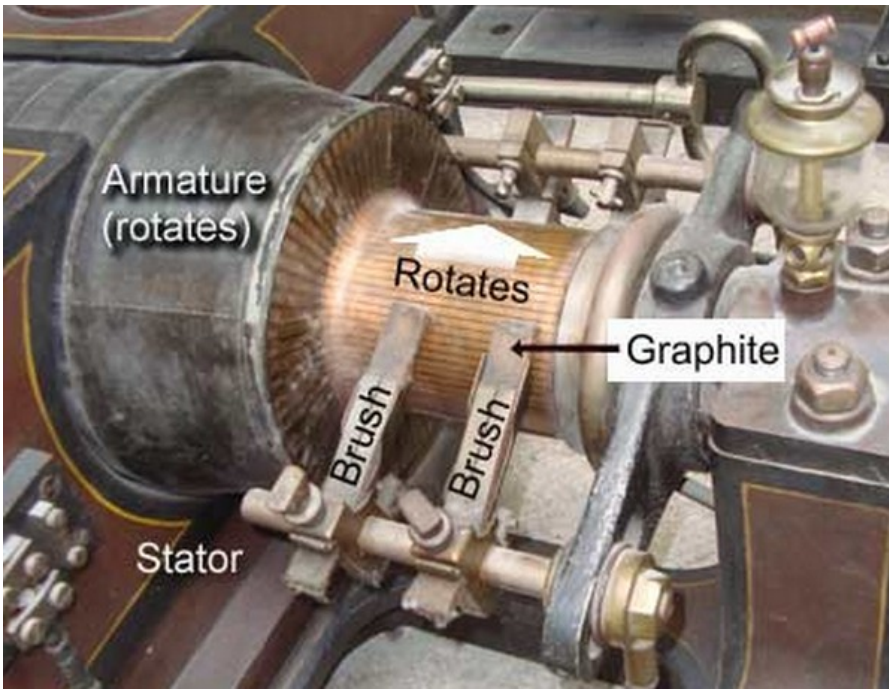

Figure 2: An example of a sliding electric contact consisting of a copper armature and graphite brushes [14]

2.2 Classification of Diamond-like Carbon

Diamond-like carbon or DLC is a thin film material that consists of either hydrogenated amorphous carbon (a-C:H) or non-hydrogenated amorphous carbon (a-C) with high fraction of metastable sp^3 carbon bonding. It is generally prepared by a deposition process that involves energetic ions which give rise to the sp^3 bonding. The sp^3 bonding is metastable compared to sp^2 bonding, unless it is stabilized by C–H bonds. The ternary phase diagram in Figure 3 was first derived by Jacob and Moller and displays the types of DLC. It can be seen that the fraction of sites in the alloy are C sp^3, C sp^2 or H [1, 15].

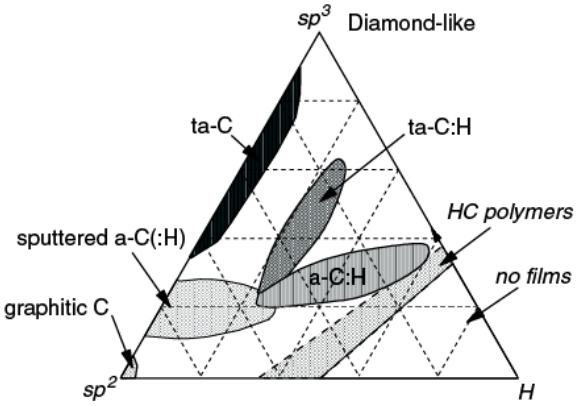

Figure 3: Ternary phase diagram of the C, H system [15]

Three main regions can be observed from the diagram. Along the left axis is the first region which is the hydrogen-free a-C region. The sp^2 a-C in this region is not a DLC. A DLC is an a-C with a higher sp^3 content but still without hydrogen and is usually made by deposition technique like unbalanced magnetron sputtering. They can contain quite large amounts of sp^3. Moving further up the axis, a specific type of a-C is encountered. This is a-C with high sp^3 content and is classified as tetrahedral amorphous carbon (ta-C). It is deposited at room temperature by ion or plasma beams with high ion fraction and narrowly defined ion energy [3, 15].

The second region is in the bottom right corner of Figure 3. The boundary line of the region is between the composition C_2H_2 on the sp^2-H axis and $(CH_2)_n$ on the sp^3-H axis. Here the hydrogen content is so large that the material can only form gas molecules and not a fully connected network.

In between the two regions lie a-C:H materials. These films are usually produced by plasma-enhanced chemical vapor deposition (PECVD) of hydrocarbon molecules, by reactive sputtering of graphite in an atmosphere including H or by ion beam deposition from a hydrocarbon gas precursor [11, 15].

2.3 Deposition Processes

The first hard amorphous carbon coatings were deposited by a beam of carbon ions produced in an argon plasma on room temperature substrates. Following this, several alternative techniques have been developed.

Amorphous carbon coatings have been produced by many different deposition methods and a variety of carbon-bearing solid or gaseous precursors. Deposition methods include evaporation, DC, RF, or ion beam sputtering, RF or DC plasma-enhanced chemical vapor deposition (PECVD), electron cyclotron resonance chemical vapor deposition (ECR-CVD), direct ion beam deposition (IBD) and pulsed laser vaporization and vacuum arc. Coatings with graphite-like properties such as very low friction, low hardness and high electric conductivity were prepared using evaporation and ion plating techniques while coatings with diamond-like properties have been produced by all of the previously mentioned techniques [2, 16–18].

Deposition technique and parameters have a great effect on the coatings structure and properties. High-energy surface bombardment as observed in cathodic arc deposition, pulsed laser vaporization, direct IBD, PECVD, ion beam sputtering, and DC/RF sputtering has been used to produce harder and denser coatings. Previous research found that sp^3/sp^2 fractions are in the decreasing order for the aforementioned methods, where carbon species arrive at the substrate with energy significantly greater than that represented by the substrate temperature, producing an energetic deposition. The coatings result in having an amorphous structure, with H content up to 50 % and a high degree of sp^3 character [3, 19, 20].

The deposition of sp^3-bonded carbon requires high kinetic energies, considerably higher than those obtained with thermal process like evaporation (0 – 0.1 eV). The depositing species have to have kinetic energies of 100 eV or higher which are then quenched into metastable configuration. Excess energy, which can be produced by substrate heating, prevents the formation of high sp^3 fraction. Higher hardness of the coatings is usually the results of a high fraction of sp^3-bonded carbon atoms in amorphous network [1, 9].

Deposition conditions have a significant impact on the sp^3/sp^2 – bonded carbon ratio, the adhesion of the coatings to the substrate and the amount of H in the coating. These characteristics dictate the coatings mechanical and tribological properties therefore the deposition rate, precursor material, kinetic energy of the carbon species prior to deposition, substrate, substrate biasing and substrate temperature have a great effect on the properties of the deposited coatings. Table 1 summarizes the processes, deposition rates and kinetic energies of the commonly used methods for the deposition of DLC coatings [21, 22].

Table 1: Summary of the most commonly used deposition techniques [22]

Deposition technique	Process	Kinetic energy [eV]	Deposition rate [nm/s]
Filtered cathodic arc (FCA)	Energetic carbon ions produced by vacuum arc discharge between graphite cathode and grounded anode	100 – 2500	0.1 – 1
Direct ion beam (IB)	Carbon ions produced from methane gas in an ion source and accelerated towards the substrate	50 – 500	0.1 – 1
Plasma enhanced chemical vapor deposition (PECVD)	Hydrocarbon species, produced by plasma decomposition of hydrocarbon gases (e.g. acetylene) are accelerated towards a DC-biased substrate	1 – 30	1 – 10
Electron cyclotron resonance plasma chemical vapor deposition (ECR-CVD)	Hydrocarbon ions, produced by plasma decomposition of ethylene gas in the presence of a plasma in electron cyclotron resonance condition, are accelerated towards an RF-biased substrate	1 – 50	1 – 10
DC/RF sputtering	Sputtering of graphite target by argon ion plasma	1 – 10	1 – 10

2.4 Doping of DLC Coatings

Significant interest for DLC coatings properties of many research groups has sparked the progression of the DLC materials by doping the coatings with various elements. The incentive was to modify the properties and nature of DLC coatings by alloying with different elements and metals, while retaining the amorphous structure of the coating. The deposition of modified DLC films is done using the same techniques as for regular DLC films with the addition of the modifying element in the deposition environment. Doping enables films properties, such as thermal stability, electrical conductivity, surface energy, biocompatibility, hardness and tribological properties, to be continuously adapted to the desired values of specific applications [1, 17, 23, 24].

DLC coatings exhibit extremely low wear rates which are usually attributed to the excellent combination of high hardness and low coefficient of friction. Nevertheless, relatively high compressive stresses can be found in DLC films. Previously, the lowering of internal stresses in the film was achieved by decreasing the energies of carbon species arriving at the substrate surface or by increasing the deposition temperature, all at the cost of reducing the sp^3/sp^2 ratio. The coatings are now doped with different metals and metallic interlayers are being used between the coating and the substrate to minimize or eliminate the compressive stresses in the coatings without reducing the sp^3/sp^2 ratio [7, 25].

The modification of DLC coatings by doping with various elements can lead to significantly improved properties and performance and thus greater multifunctionality in practical applications. Most modifications have been made to reduce their, typically high, internal compressive stresses, to increase the adhesion to the substrate (N, Si, metal incorporation), to alter electrical properties (Me-DLC), to modify surface energy (N, F, O, Si) or to increase their biocompatibility (Ti, Si, Ca) [1, 25–27].

2.5 Multilayer DLC Coatings

Doped elements in DLC coatings can either be diluted in the matrix and a new single phase coating is produced or they can be present as a second separate phase modulated in the nanometre scale. The nanocomposite and multilayered films belong to the latter which is a new category of advanced nanostructured coatings. The proper control of the coatings structure and composition at the nanoscale enables the possibility for new improvements of the coatings. Properties such as enhanced hardness, fracture toughness and adhesion to the coatings can be improved by these new structures. This leads to enhanced wear resistance of the modified films. Various multilayering concepts are shown in Figure 4 [1, 25].

Multilayered coatings are being extensively researched as a possibility to improve the properties of DLC or reduce the undesirable properties while preserving the favorable properties of pure films. Multilayers have been known to reduce grain growth and limit crack propagation which in turn increases the coatings toughness. The periodicity of the multilayer structure also effects the tribological properties with shorter periods promoting wear resistance and longer periods promoting fatigue resistance [15, 25, 28].

Obtaining a nanocomposite film morphology consisting of a high density of nanometer-sized crystals embedded in an amorphous matrix is another possibility of enhancing the properties of DLC coatings, as for instance, titanium or wolfram carbide particles in an a-C:H matrix. This type of film contains significantly larger grains, as opposed to the ultra-hard nanocomposites. The grains measure some tens of nanometers with a thicker amorphous phase of about 5 nm, that separates the nanocrystallites.

The size of the crystallites is large enough, around 10 ± 50 nm, to enable the formation of dislocations, but too small for self-propagation of cracks. The larger separation of grains enables the adaptation of incoherency strains and allows the formation of nanocracks between the crystallites. This leads to pseudoplastic behavior which displays higher toughness and hardness values. In a case of a nanocomposite TiC film, it exhibited four times higher toughness than single-crystalline Ti-C with hardness values of around 32 GPa [25, 29–31].

Current knowledge of nanostructured films enables the development of new coatings and tailoring their properties to specific tribological requirements of the applications, by controlling the microstructure and chemical composition at the nanoscale [8, 9].

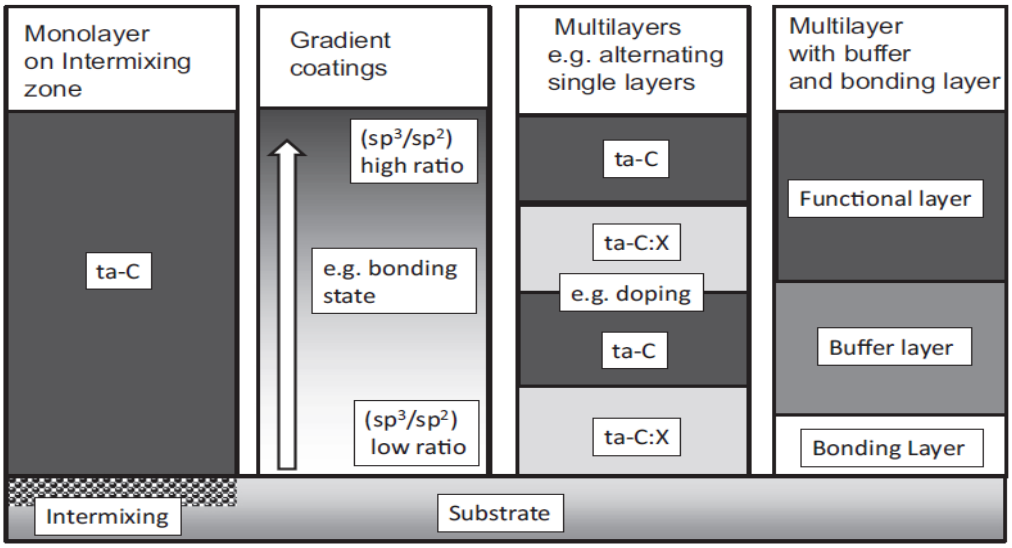

Figure 4: Basic multilayer concept, gradient coatings and "pseudo" multilayers for undoped and doped a-C coatings [9]

2.6 Mechanical properties

The great variety of DLC structures and compositions leads to a wide range of mechanical properties. Hardness varies from a few GPa for a-C up to more than 60 GPa for ta-C. The same trend is seen for the elastic modulus ranges where it spans from several tens of GPa for a-C to up to several hundreds of GPa for ta-C. For both a-C and ta-C, there is a tendency towards a decrease in hardness and elastic modulus with the increase of hydrogen content. On the other hand, higher sp^3 fraction content improves these mechanical properties. It could be said that DLC films are harder than most metallic materials [3, 9, 32].

High hardness/elastic modulus ratios were also observed for DLC films which means that they are relatively strain tolerant. It has also been observed by other researches that highly hydrogenated a-C:H films exhibit excellent relaxation abilities, probably due to some free volumes in their structures. High wear resistance and low friction of DLC coatings can be attributed to the combination of excellent mechanical properties with weak surface interactions. These excellent properties and the wide range of tribological applications have prompted researches to further deepen their understanding of growth mechanisms, surface chemical and physical states, and tribological behaviors [5].

Regardless of their excellent tribological properties, high wear resistance and low friction under various sliding contact conditions, it must be noted that the coatings do have some constraints.

The environmental species and conditions of use can dramatically affect the performance of the films. High residual stresses and consequent adhesion failures are also pointed as one of the major limitations of both a-C and a-C:H coatings [1, 19, 26].

This led to various customizations such as doping of DLC coatings with additional elements, changing the coatings structure and adjusting the deposition parameters, to try and overcome the restrictions of DLC coatings and provide the necessary multifunctional requirements for future tribological applications. It was indicated by several researches that the addition of metals such as Ti, W, Cr, Zr, Cu or Ag, to the films could reduce residual stress and subsequently minimize the risk of premature coating adhesion failure [17, 26, 30, 33]. A summary of methods for tailoring the coatings properties is shown in Figure 5.

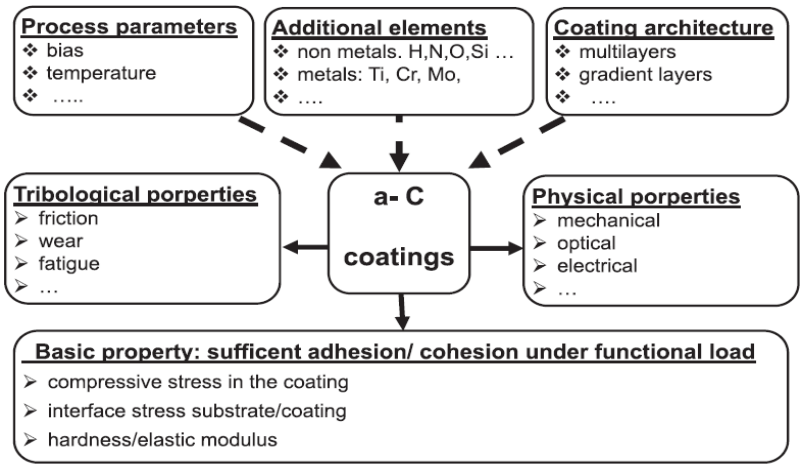

Figure 5: Methods for tailoring coatings and their properties [9]

2.7 Electrical Properties

Electrical resistance is the basic property of materials when considering their electronic applications. The electrical properties of DLC coatings can vary from that of a semiconductor to that of a wide band-gap insulator [34, 35]. They are determined by impurities, doping elements, bonding states (sp^2/sp^3), structure, and growth defects. The resistance of the coatings is also influenced by process parameters including ion energy and incident angle, substrate temperature, deposition rate [9]. DLC films do not behave like typical semiconductors, despite having a modest band-gap [7]. The coatings electrical properties have been modeled assuming a band structure consisting of only a mobility gap, where carriers residing in gap states are localized. This mobility gap produces semiconductor behavior, however, the high density of localized gap states leads to low apparent carrier mobilities and significantly degrades the semiconducting properties of materials. The mobility at room temperature of DLC has been found in the range of 10^{-11} – 10^{-12} cm^2/V. The coatings are generally characterized by high electrical resistance spanning a large range of values, from 10^2 to 10^{16} Ωcm [36].

The factors that influence the films electrical properties could be summarized as following:

- Structure – The ratio between sp^3 and sp^2 fractions present in the coating.
- Method of film preparation – Depending on the deposition conditions employed, structural and electronic defect concentrations, dislocation densities, porosity content, density, chemical composition and stoichiometry, electron trap densities, contact etc., result with electrical property implication.

- Doping elements and impurities – Effect on the bonding state (sp^3/sp^2), dopant induced graphitization and conduction mechanism.
- Degree of film continuity – Conduction mechanisms in discontinuous, island structure films differ from those in continuous structure films.
- Size effect – Surface scattering and quantum mechanical tunneling of charge carriers.
- High chemical reactivity – Corrosion, absorption of water vapor, atmospheric oxidation and sulfidation, and low-temperature solid-state reaction changes in electrical properties.

  [34, 36–39]

2.7.1 Effects of Structure, Deposition Methods and Doping Elements on Electrical Properties of DLC Coatings

In the last two decades, substantial research has been done related to electrical properties of DLC coatings and how different structures, deposition methods and doping with various elements can alter electrical properties of the coatings. The many possible applications of DLC coatings in electronic devices would further develop by knowing in detail how the coatings characteristics influence electrical properties of the coatings and tailoring them to specific needs [40].

The sp^3/sp^2 hybridization ratio is considered as the most important parameter to characterize DLC coatings and has a great effect on the electrical properties of DLC coatings [41]. Nakayama et al. [42] measured the electrical resistance of a-C:H and a-C:N as a function of hydrogen and nitrogen content. For a-C:H films, they reported an increase of electrical resistance with the increase of hydrogen content. At low hydrogen contents, the structure has a conductive graphite-like structure due to the sp^2 bonding. With greater hydrogen content, structure changes to sp^2 clusters embedded in sp^3 bonded matrix. With a further increase of hydrogen in the film, the sp^2 clusters get smaller, while sp^3 bonding increases, giving the film a less conductive diamond-like structure. Nitrogen incorporation in a-C:N films changes the structure by bonding with carbon and forming sp bonding of C≡N and sp^2 bonding of C=N, together with sp^3 bonding of NH_2. Low nitrogen contents (at.% < 7 %) showed a decrease in the film resistance indicating a high graphitic content. The lowest resistance was observed for nitrogen at 10 at.% concentration in the film which was attributed to the conductive nature of sp^2 bonding of C=N. The nitrogen acts as a thermally activated impurity center in graphitic structures and contributes to the electrical conductivity, but at high nitrogen contents the resistance increases up to two times its magnitude inducing a change in the microstructure to pyridine-like structures and nitrile bonds. Thus, at high N content, these bonds break the interconnection of the graphitic structure of the film and reduce the conduction path of the carriers [4]. Nitrogen doped regimes from 0.4 % - 10 % make the existing sp^2 sites condense into clusters and reduce the band gap. Nitrogen contents over 10 % change the bonding from sp^2 to sp^3 drastically. It was concluded that the dopant induced structural changes in the films, resulting in different ratios of sp^3/sp^2, caused the increase or decrease of electrical resistance of the coatings depending on the amount of dopant. The results of the study are presented in Figure 6. Guerinoa et al. [32] analysis of nitrogenated DLC films came to similar conclusions that low amounts of nitrogen increase the conductivity of DLC film while higher amounts strongly reduce it.

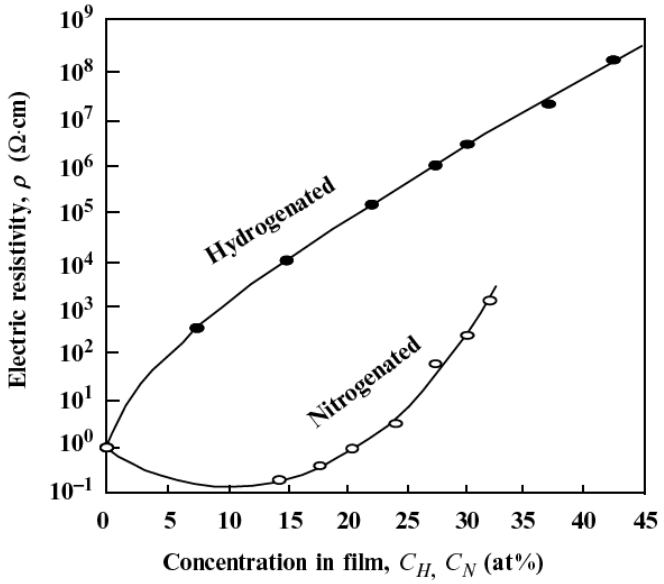

Figure 6: Relation between electric resistance and hydrogen / nitrogen content in DLC films [42]

Doping of DLC films has also been done with many different metals including Ti, Nb, Ta, Cr, Mo, W, Ru, Fe, Co, Ni, Al, Cu, Au, Ag. The advantage of Me-DLC films as electronic materials is that the conductivity behavior can be varied from those of dielectric to those of metallic materials [43, 44]. Metals are assumed to be incorporated in the coatings as small nanocrystallites of pure metal or metal carbide, which are dispersed throughout the carbon network [26]. Four-probe measurements done by Dikshit et al. [45] revealed how dopant concentration and resistance of DLC do not change linearly. Usually, amorphous semiconductors have all states localized and exhibit hopping conduction mechanisms. With the increase of dopant concentration, the distance that the electron will cross over one tunneling event would decrease which would subsequently lead to lower resistance. When the dopant concentration is high enough, for continuous channels to be formed for the transportation of electrons. the coating could display metallic like behavior. For instance, DLC films containing 15 % Ta, W, Ti, Nb have been deposited by DC magnetron sputtering of the metals in acetylene and have similar wear resistance as DLC and friction coefficients < 0.2, but higher conductivity (up to 5 mΩcm) [36, 42]. Wei et al. [25] have measured the I-V characteristics of Ti doped DLC and concluded that Ti–C bonding present in the film is essentially metallic and the presence greatly enhances the conductivity of the coating. Suzuki et al [46]. were developing electrically conductive DLC coated stainless steel separators for polymer electrolyte membrane fuel cells and found that when simultaneously implementing boron and nitrogen ions into the DLC coating, the electrical properties changed from that of an insulating film to a conductive film with electrical resistance of less than 5 mΩcm. Endrino et al. [30] also studied the influence of different metals (Au, Ag, Cu, Mo) incorporated in DLC films. They reported a drastic increase in conductivity together with a decrease in band-gap when films were doped with metals. They also concluded that the host matrix was predominately graphitic and was not affected by metal impurities, except for Mo, where the formation of carbides was observed.

Structure of DLC coatings and their electrical properties strongly depend on the deposition conditions as well. In general, the conductivity of DLC films may change in the range of over ten decades depending on the deposition conditions. There are many different deposition methods for depositing DLC films. Main factors that influence the resistance of the films are RF power, substrate temperature, bias voltage, RF method and precursor gases [36, 47]. Electrical resistance of the coatings is also strongly influenced by the carbon ion energy in ion beam depositions. Higher ion energies reduce the sp^3 content and generate again more sp^2 bonding, thus the electrical resistance drops [9]. Staryga and Bak [35, 41] reported that as the power density increases, the resistance of DLC films decreases. When the gas pressure was held constant, the conductivity increased with increasing negative self-bias voltage. The conductivity increased by nearly eight orders of magnitude at room temperature with increasing self-bias voltage. The value of the self-bias voltage itself did not determine the structure of obtained films entirely, but it has been shown that the amount of hydrogen decreases and the sp2 fraction increased with increasing value of the self-bias voltage. Vetter [9] reported a dramatic drop in resistance with substrate temperature during deposition, from around 108 Ωcm at -100°C to 1 Ωcm at 450°C. Honglertkongsakul et al. [38] also reported a decrease in resistance with increasing substrate temperature at a constant laser fluence in pulsed laser deposition. At constant temperature, the conductivity increases with increasing laser fluence. Miyagawa et al. [40] studied the resistance of coatings deposited by plasma-based ion implementation with bipolar pulses. The results showed that the resistance of the films decreased with pulsed negative voltage and reached 1 mΩcm at -20kV. In the research of DC PACVD deposited DLC films, Grill et al. [36] concluded that the resistance of the film is determined by substrate bias and to be precursor dependent. A summary of different deposition methods and their reported electrical resistance are summarized in Table 2.

Table 2: Electrical properties of different materials and DLC coatings deposited by various deposition methods [9, 38, 48]

Material / coating	Electrical resistance [Ωcm]
Diamond	$10^{7} – 10^{20}$
Graphite	5×10^{-5}
Glassy Carbon	$10^{-2} – 10^{-3}$
a-C evaporation	$10^{-1} – 10$
a-C sputtering	$10^{-1} – 10^{5}$
a-C:H PECVD	$10^{7} – 10^{14}$
a-C:H Ion	$10^{7} – 10^{14}$
a-C FCVAE	$10^{2} – 10^{3}$
a-C PLD	$10^{4} – 10^{5}$

When two materials are in contact, the collective resistance is not only dependent on the resistance of the materials, but also on the resistance of the contact. The resistance of the contact could be affected by various contact properties such as the formation of oxide layers, real contact surface area, operating conditions (sliding). Ultimately the resistance of the contact can be substantially higher compared to the independent resistance of the materials in contact. That is why the research in this work was focused on evaluating the electrical properties of the coatings during tribological testing with the addition of electric current.

3. Experimental Methodology

3.1 Materials

Materials used in this research were Ti-DLC coatings, W-DLC coatings and 100Cr6 Steel. The coatings were selected based on preliminary testing and commercial availability of the coatings. During preliminary testing, measurements of surface dielectric properties of different DLC coatings were performed. Measuring was done on a Hameg 8118 instrument, connected to the circular electrodes on the surface with the following experiment conditions: 3 V applied voltage and AC in the frequency range of 60 Hz – 60 kHz. Measuring setup can be seen in Figure 7.

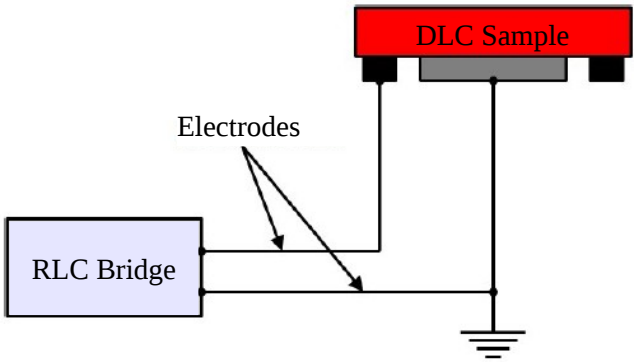

Figure 7: Surface dielectric properties measuring setup diagram [49]

Results of the study, presented in Figure 8, show the complex surface conductivity of the samples. Based on the results, the coatings were divided into two groups, the semi conductive and the conductive coatings. The coatings determined as conductive were Tetrahedral carbon, Ti-DLC, Low W-DLC and High W-DLC.

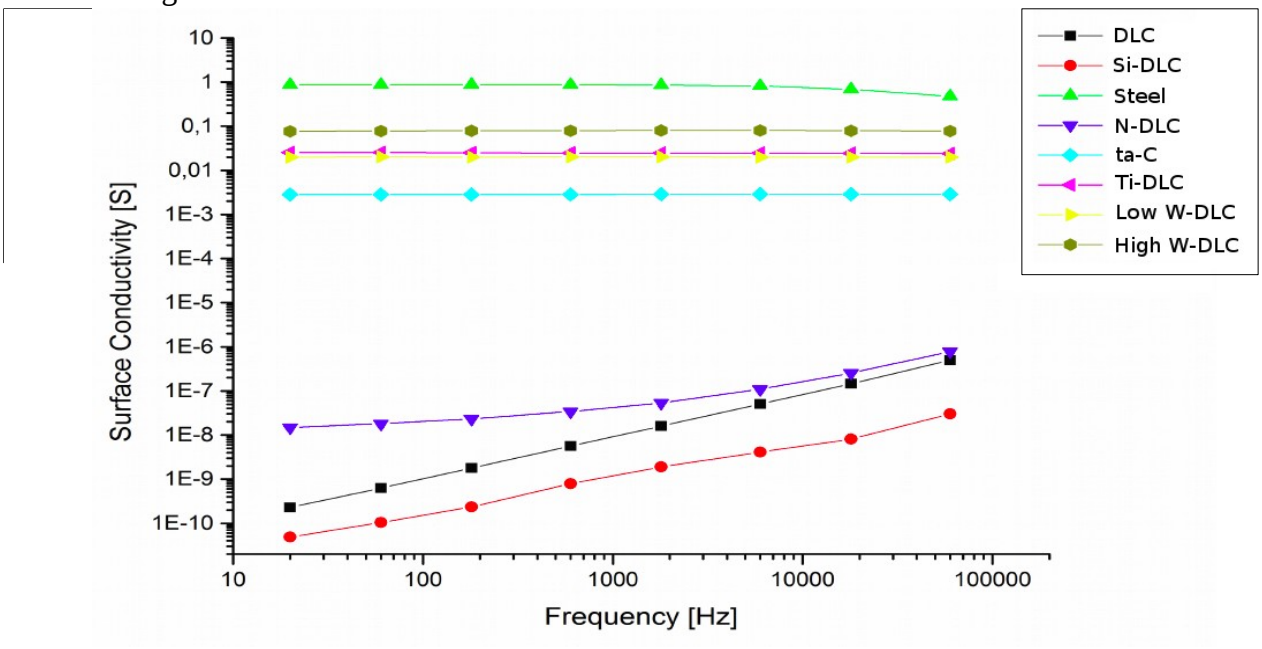

Figure 8: Complex surface conductivity of various DLC samples [49]

Following the results of study of surface conductivity and commercial availability, Ti-DLC and W-DLC were selected as the most promising coatings with their relatively high conductivity in relation to other DLC samples. 100Cr6 Steel, known for its high conductivity, was used as a reference material in order to compare DLC coating and steel conductivity behavior. Four types of doped coating samples, presented in Table 3, were used in the experiment.

Table 3: Types of sample coatings and amount of doped element

Type of coating	Amount of doped element
Low Ti-DLC	5 at.% Ti
High Ti-DLC	10 at.% Ti
Low W-DLC	5 at.% W
High W-DLC	10 at.% W

The aim of the research was to compare commercially available DLC coatings, therefore the sample coatings were in “as supplied” state, without any special treatments or alterations. As DLC coatings are almost never deposited directly on the substrate, in our case steel, there is an interlayer present between the substrate and the coating. The effects and contributions of the interlayer to the conductivity of the coating were not separately analyzed.

Test specimens were provided as circular pieces (discs) with dimensions of 25 mm diameter and 10 mm thickness and balls with a diameter of 10 mm. The coatings were deposited on 100Cr6 samples with a thickness in the range of 1 – 2 μm. All surfaces were polished to a smooth surface finish, Ra of 0.05 μm.

Sample materials were tested in different combinations. Table 4 shows the combinations of materials, that were tested.

Table 4: Test material combinations

Ball sample	Steel	Steel	Steel	Steel	Steel
		Low Ti-DLC	High Ti-DLC	Low W-DLC	/
Disc sample	Steel	Low Ti-DLC	High Ti-DLC	Low W-DLC	High W-DLC

3.2 Test Equipment and Procedures

For the purpose of the experiment, a specific setup was employed to simultaneously measure the electrical and tribological properties of the coatings under stationary and dry sliding conditions.

3.2.1 Characterization of Tribological Properties

A CETR UMT-2 (CETR now owned by Bruker, USA) tribometer with the DFH-20-0758 sensor and a hard spring was employed for the evaluation of the tribological properties. The hardware configuration of the tribometer is presented in Figure 9 (b). The test utilizes a flat lower sample and a ball-shaped upper sample. The samples slide relative to each other in a linear, back and forth sliding motion under predetermined test conditions. The load is applied vertically through the ball against the lower flat disc sample. The tests were done in constant load reciprocating sliding. Test parameters, such as load, oscillating frequency and duration of test are set through UMT software arranged in test steps and sequences. The software enabled continuous data collection of friction force, normal force and time. The coefficient of friction (COF) was automatically calculated by the software using normal force and friction force data. Sampling rate was set at 10 measurements per second. Components of the measuring setup, utilized to obtain tribological properties, are shown in Figure 9 (a). The prescribed set of test parameters for all tests are presented in Table 5.

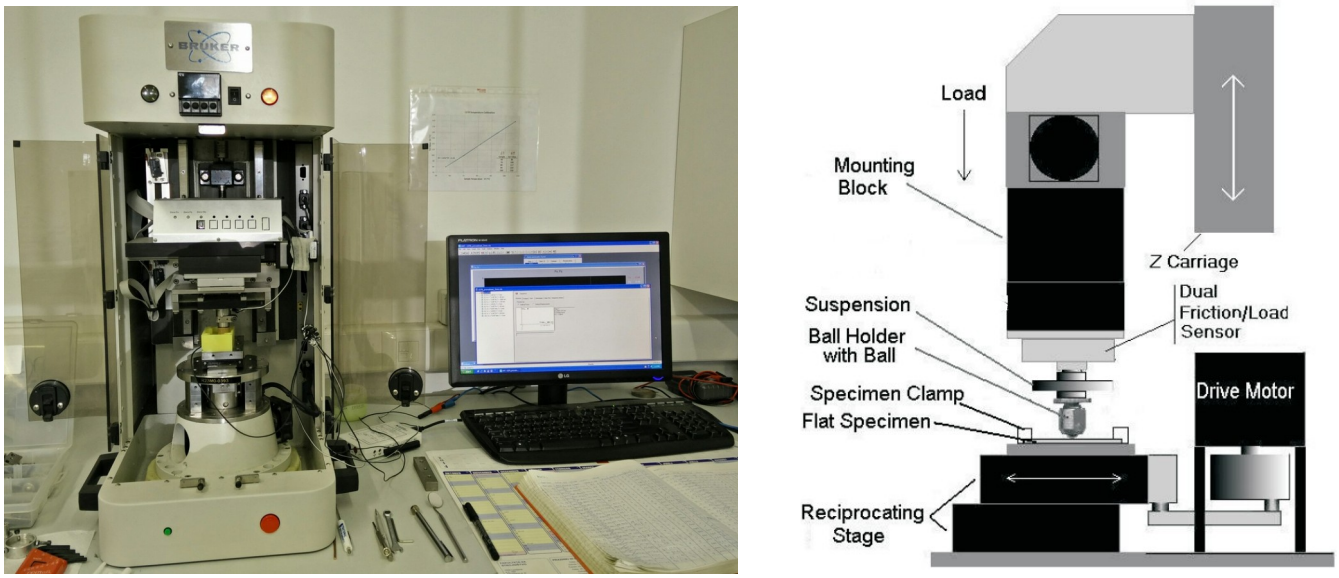

(a) *(b)*

Figure 9: CETR UMT-2 connected to a computer with UMT software (a) and its hardware configuration scheme (b) [50]

Table 5: Test parameters

Applied load	3 N
Stroke length	5 mm
Oscillating frequency	5 Hz
Temperature	Ambient (around 24°C)
Duration	1000 s
Combined sliding distance	100 m
Lubrication	None

3.2.2 Characterization of Electrical Properties

Characterization of electrical properties for the selected samples was done by evaluating their conductivity in stationary and sliding conditions. Conductivity was estimated by measuring the voltage drop at a predetermined constant current in the ball – disc contact. Voltage drop was measured between when the samples were detached (open circuit) and when they came into contact (closed circuit). Greater the voltage drop (lower the measured voltage), higher the conductivity of the material in contact.

A custom setup, displayed in Figure 10, was compiled in order to carry out the electrical conductivity measurements required for the research of the electrical properties of the samples. The following components of the measuring setup were employed to obtain the electrical properties:

- Programmable DC power supply Tektronix PWS4323
- Data acquisition device NI myDAQ
- LabView data logging and analysis software
- Insulated sample holder

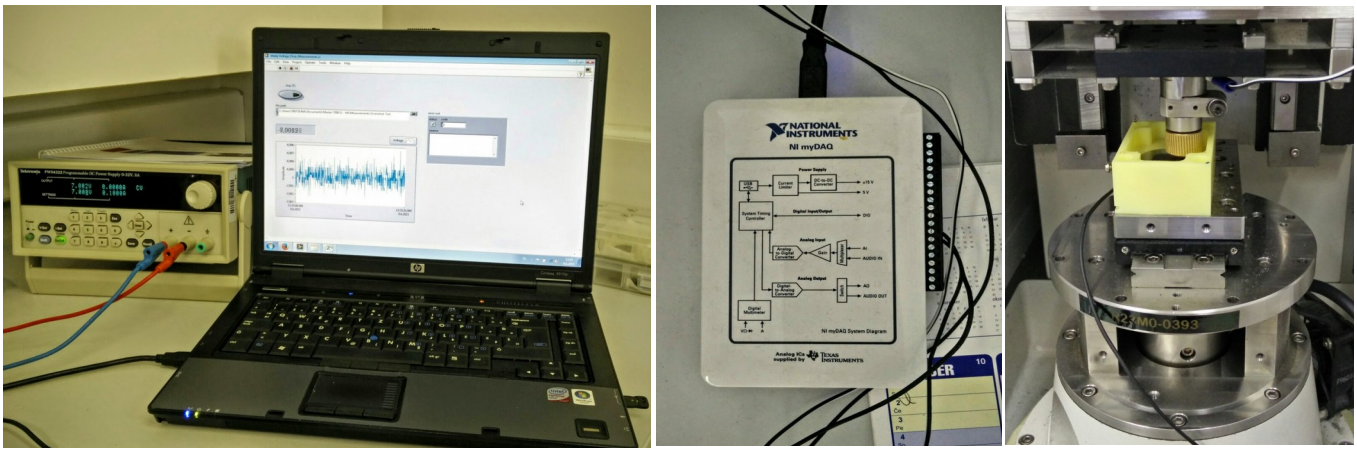

(a) *(b)* *(c)*

Figure 10: DC power supply and LabView software (a), NI myDAQ (b) and insulated sample holder mounted on CETR - UMT2 (c)

Electric circuit needed to acquire data for the analysis of contact resistance of the test subjects was rather simple. DC power supply was connected in series directly to the surfaces in contact. One of the terminal wires was connected to the ball holder, which was already insulated from the rest of the device. The other terminal wire was attached to a copper plate incorporated in the insulated holder under the sample. Insulation of the samples from the rest of the device was necessary in order to ensure the current passed through the samples and not the surrounding components. The data acquisition device was connected parallel to the power supply and the samples. The electric circuit schematic is shown in Figure 11. The data acquisition device was connected to a computer through USB. The processed data was displayed and continuously logged by the LabView software program (Figure 12). Sampling rate was 100 measurements per second. Logged data was then imported into Libreoffice Calc for final analysis.

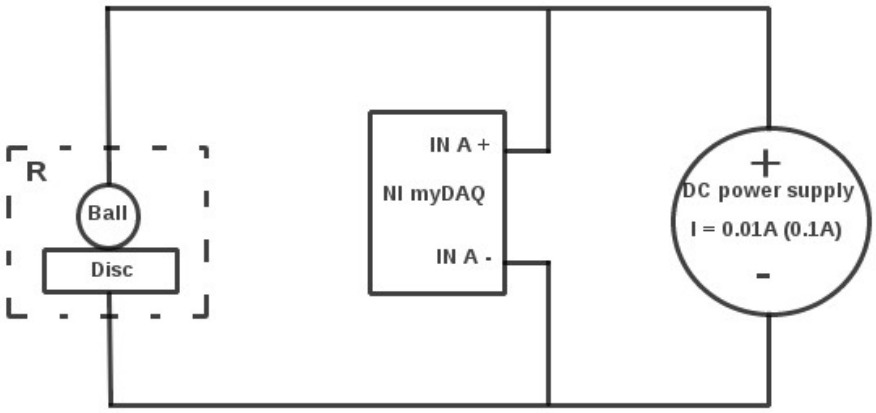

Figure 11: Electric circuit diagram

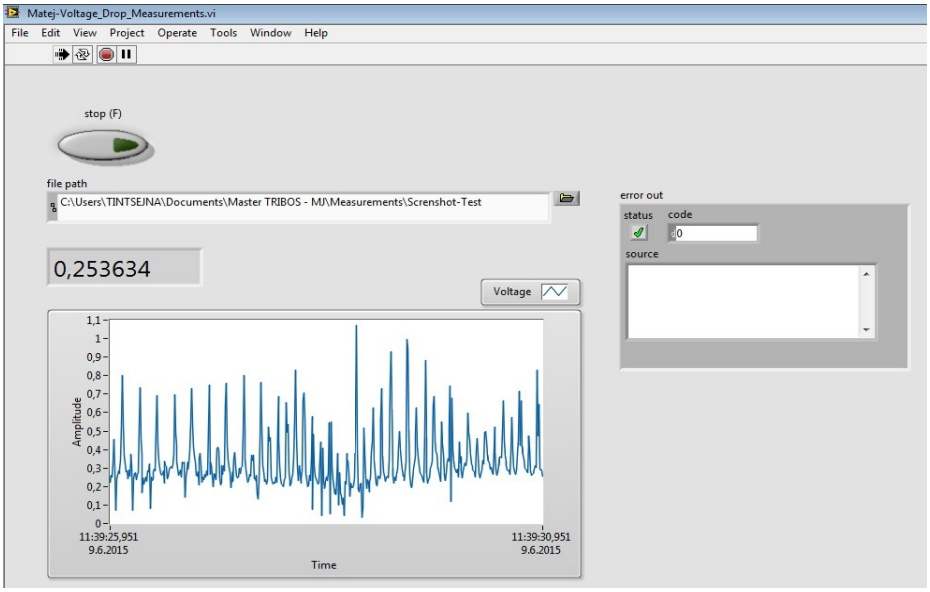

Figure 12: LabView program for voltage drop data logging

3.2.3 Analysis of Wear Scars

Two different microscopes, displayed in Figure 13, were used for the analysis of wear scars on the ball and disc samples. Before the analysis under the microscope was performed, the sample surfaces were cleaned with 2-propanol solution.

A Nikon Eclipse LV150 optical microscope (Nikon, Japan) paired with NIS – Elements D3.2 software was used to investigate the worn surfaces of the ball and disc samples. It gave an insight on how wear differentiated between individual test conditions.

3D optical microscope Bruker Contour GT (Bruker, USA) through white light interferometry and coupled with Bruker Vision 64 software allowed for additional review of the wear scar depths and their topography. Only disc sample wear scars were investigated under 3D optical microscope. The wear track profile data was imported and analyzed with Libreoffice Calc software.

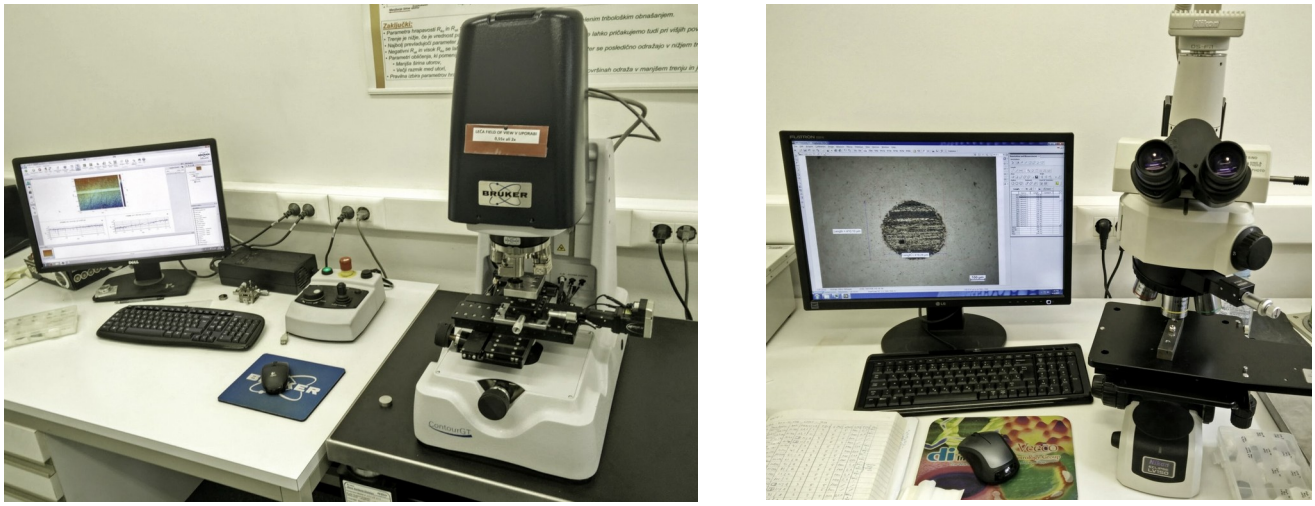

(a) *(b)*

Figure 13: 3D optical microscope Bruker Contour GT (a) and optical microscope Nikon Eclipse LV150 (b)

3.3 Test Procedures

Tests were performed under the following current conditions:

- No current
- I = + 0.01 A
- I = - 0.01 A
- I = + 0.1 A
- I = - 0.1 A

Negative and positive electric currents were induced by alternating the power supply terminals. Current was marked as positive, when the positive terminal from the power supply was connected to the ball sample and the negative terminal to the disc sample. Current was marked as negative, when the conditions were reversed (ball – negative terminal, disc sample – positive terminal).

There were two types of tests employed, one where different electric currents were present and the other in the absence of electric current. Minimum of two measurements were done for each combination of materials and applied current to ensure the consistency of the results. If the results of the first two measurements of a certain combination of materials and electric current were not showing a certain uniformity, additional tests were performed in order to either confirm the data collected was accurate or to amend the results with representative measurements.

Two different test sequences were used for when electric current was applied and when there was no electric current present. Measuring sequence without electric current provided only the coefficient of friction data during sliding. Measurements with applied electric current provided voltage drop data for static and sliding conditions. Static voltage drop measurements were done in different conditions. First voltage drop measurements were done after loading the contact, before sliding was initiated to measure the resistance of unused surfaces. After the sliding stopped, the samples remained in contact for 120 seconds, to obtain voltage drop measurements of the worn surfaces. The samples were then detached and joined back together for 60 seconds to observe if there were any changes in the voltage drop when reattaching the surfaces in the same spot on the sample. Following was detachment and reattachment of the samples for another 60 seconds in a new spot. This time, a fresh disc sample surface was joined with the worn ball sample surface to again observe changes in the voltage drop between different surfaces in static contact. COF was measured only during sliding as in the sequence without electric current. Presented data of voltage drop and coefficient of friction were averaged to 1 measurement per second to provide a better visual presentation of the measurements. In total, 91 tests were carried out to obtain measuring data for all material combinations and currents.

Due to the characteristic of ball – plane contact, high pressure and high current density were expected to be present. In order to ensure that there was no coating damage caused by excessive contact pressures or high current densities in the sliding contact, relatively low currents and loads were employed during testing. Maximum contact pressure was approximated using Hertzian contact theory for a sphere – plane contact. Young's modulus was estimated at 213 GPa and Poisson's ratio of 0.29. Current density was calculated by dividing the applied current with the contact area. Approximated current density and maximum contact pressures for the chosen electrical current conditions are presented in Table 6.

Table 6: Current density and mean contact pressure of ball – disc contact for selected electric current conditions

Electric current [A]	Contact radius [mm]	Maximum contact pressure p_{max} [GPa]	Current density [A / mm²]
± 0.01	0.06	0.43	0.88
± 0.1	0.06	0.43	8.8

The appropriate test parameters were determined during preliminary testing of the coatings. Wear scars were analyzed under optical and 3D optical microscopes to observe the worn surfaces and to make sure no rupture of the coating occurred. Due to software limitation, the color scale in 3D images of wear profiles could not be set to a fixed value and exported, therefore the 3D figures serve more as a visual representation of the wear tracks, and not as a comparing tool between different wear scars.

3.3.1 Test Procedure without Electric Current

Samples were mounted into their respective holders and the surfaces of the samples were cleaned with a solution of 2-propanol. Tribometer test sequence was initiated through the UMT program. The sequence was divided into the following steps:

- Ball sample lowered towards the disc sample until a contact with a normal load of 3 N was reached
- Reciprocating sliding for 1000 s at 5 Hz and 5 mm stroke length
- After 1000 s, the ball sample was raised and the test sequence ended

The samples were then removed for the analysis of wear scars under optical and 3D optical microscopes.

3.3.2 Test Procedure with Electric Current

As in the test procedure with no current, samples were mounted into their respective holders and the surfaces of the samples were cleaned with a solution of 2-propanol. Voltage drop measuring was started and the tribometer test sequence was initiated, divided into the following steps:

- Ball sample lowered towards the disc sample until a contact with a normal load of 3 N was reached
- The samples remained stationary for 60 s
- Reciprocating sliding for 1000 s at 5 Hz and 5 mm stroke length
- Additional 120 s in contact under normal load, after reciprocating sliding stopped
- Ball raised and lowered back in contact under normal load of 3 N to the same spot for 60 s
- Ball raised and moved for a 1 mm offset left and lowered back in contact onto a new surface spot under normal load for 60 s
- Ball sample raised and the test sequence ended

After the test sequence was finished, the samples were removed for the analysis of wear scars under optical and 3D optical microscopes.

4. Results and Discussion

The electrical and tribological properties of different Ti-DLC, W-DLC coatings and 100Cr6 Steel were evaluated in this research. The results are presented in the following subsections.

4.1 Steel

4.1.1 Steel – Steel

Friction and Resistance Analysis

Friction and resistance data for Steel – Steel contact is presented in Figure 14. The coefficient of friction curves show similar behavior for all electric current conditions; COF between 0.7 – 0.9 in steady state conditions. This is in accordance with the COF for Steel – Steel contact reported by other researches. No specific influence of electric current on the COF of Steel – Steel contact was observed. The resistance was however affected by the sliding. Voltage drop data were collected during static and sliding conditions. The voltage drop curves shown in Figure 14 (b) reveal how the resistance changes between steady state and sliding conditions. The voltage drop rose to 0.2 – 0.6 V, depending on the electric current applied. A varying voltage drop can be observed for both positive electric current conditions. Negative electric current conditions show a more steady voltage drop. Static voltage drop measurements immediately after sliding showed quite a difference between the different current conditions. Higher resistance was observed when positive current was applied. The difference in the voltage drop after sliding could also be attributed to different amount of oxidation of the worn surfaces in contact, detected during the optical microscope analysis. An interesting event was observed for the negative electric current conditions in the last measuring step. In both current situations, 0.01 A and 0.1 A, when reattaching the worn ball sample surface with an unused disc sample surface, there was no current flowing through the contact. This could be attributed to the severe oxidation of the worn surface observed during surface analysis, which acts as an insulating film and current can not flow through. The difference between reattaching the worn surfaces of both samples and reattaching one used and one unused surface of the samples could be in the conformity of asperities in contact. When the worn surfaces were reattached, the asperities aligned back in the foregoing positions, forming a contact between the previously exposed surfaces to enable current conduction. With the reattachment of the worn ball sample surface with an unused surface, only the oxidized asperities came in contact with the fresh surface, thus preventing electrical conduction.

Surface Analysis

Wear scars on the surface of both counterparts were analyzed using an optical microscope. The wear track profiles presented in Figure 15 correspond to the width and depth of the wear scar. It can be seen from the following figures that the wear is quite severe on both counter parts. This was expected as unlubricated Steel – Steel contact is known for high friction and wear rates. As mentioned before, electric current did not have any significant effect on wear or COF. On the worn surface of the ball sample in Figure 16, the oxidation of the surface that presumably obstructed the conductivity of the sample can be observed.

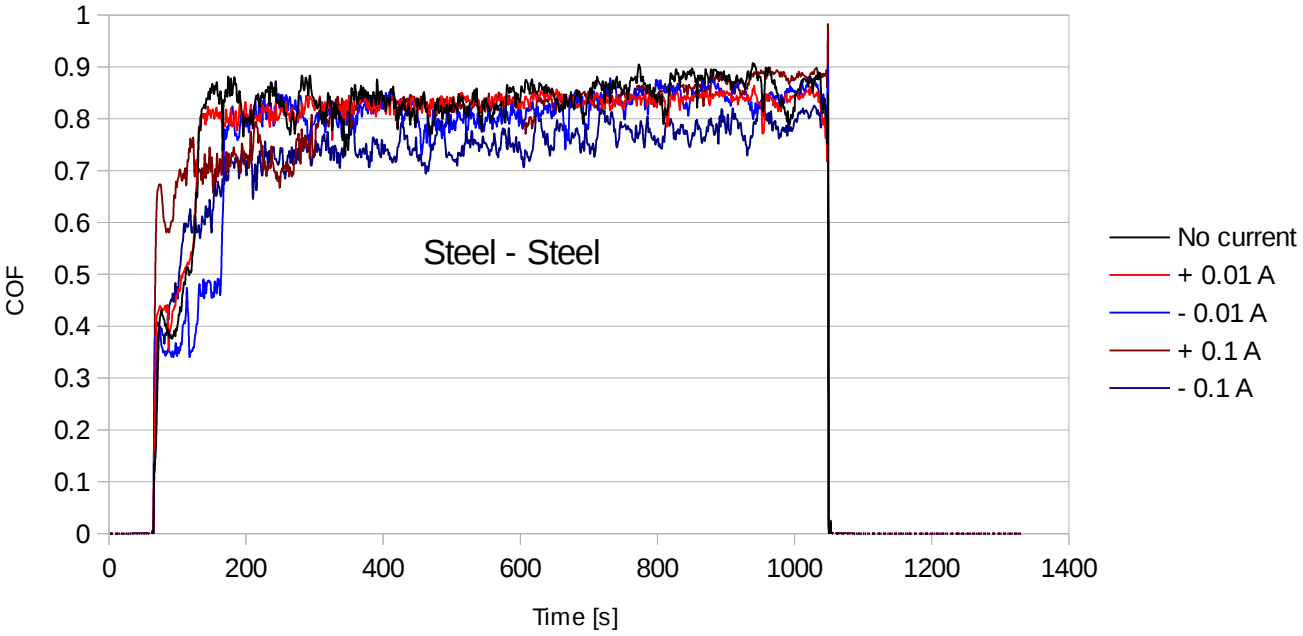

(a)

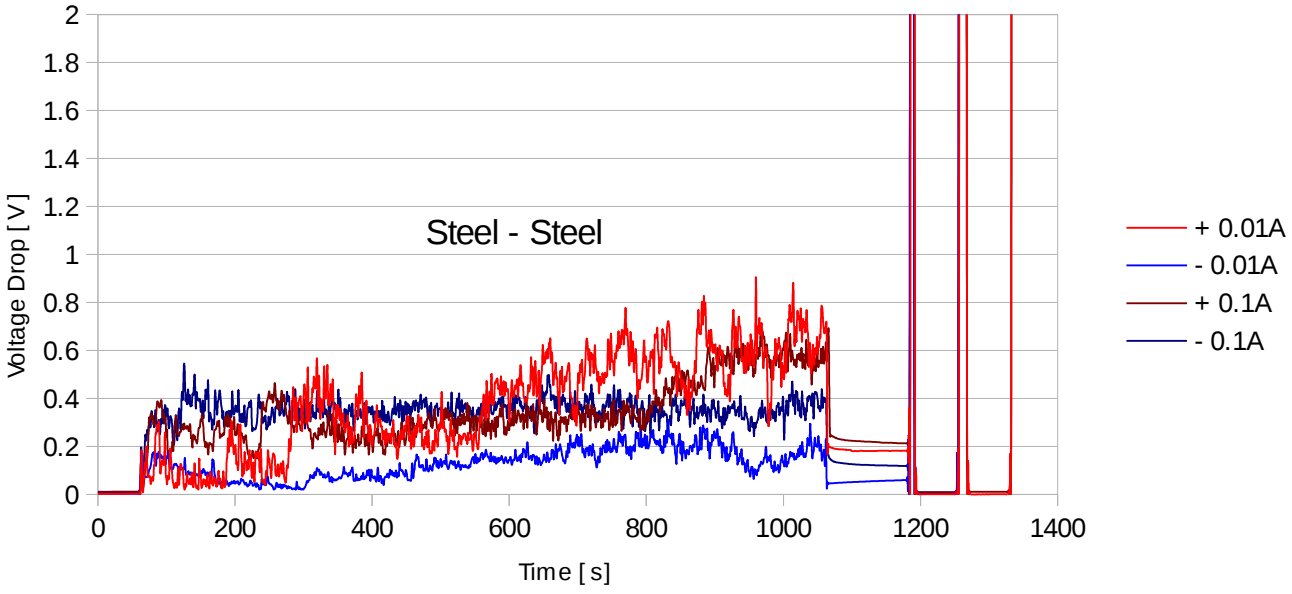

(b)

Figure 14: Coefficient of friction (a) and Voltage drop (b) of Steel – Steel contact

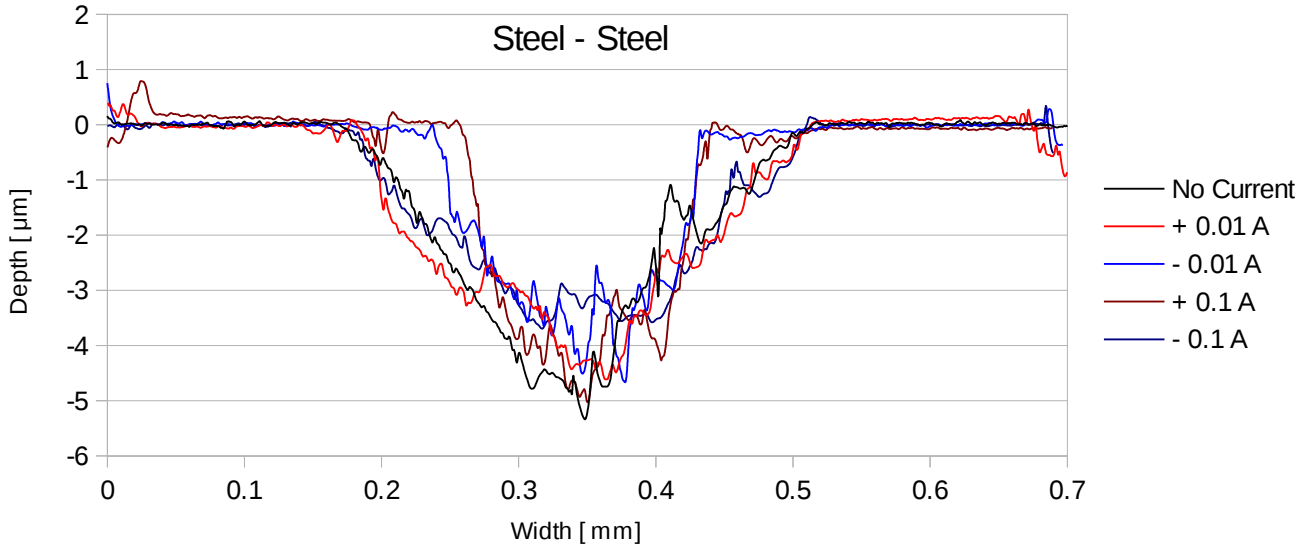

Figure 15: Wear scar profiles of Steel – Steel contact

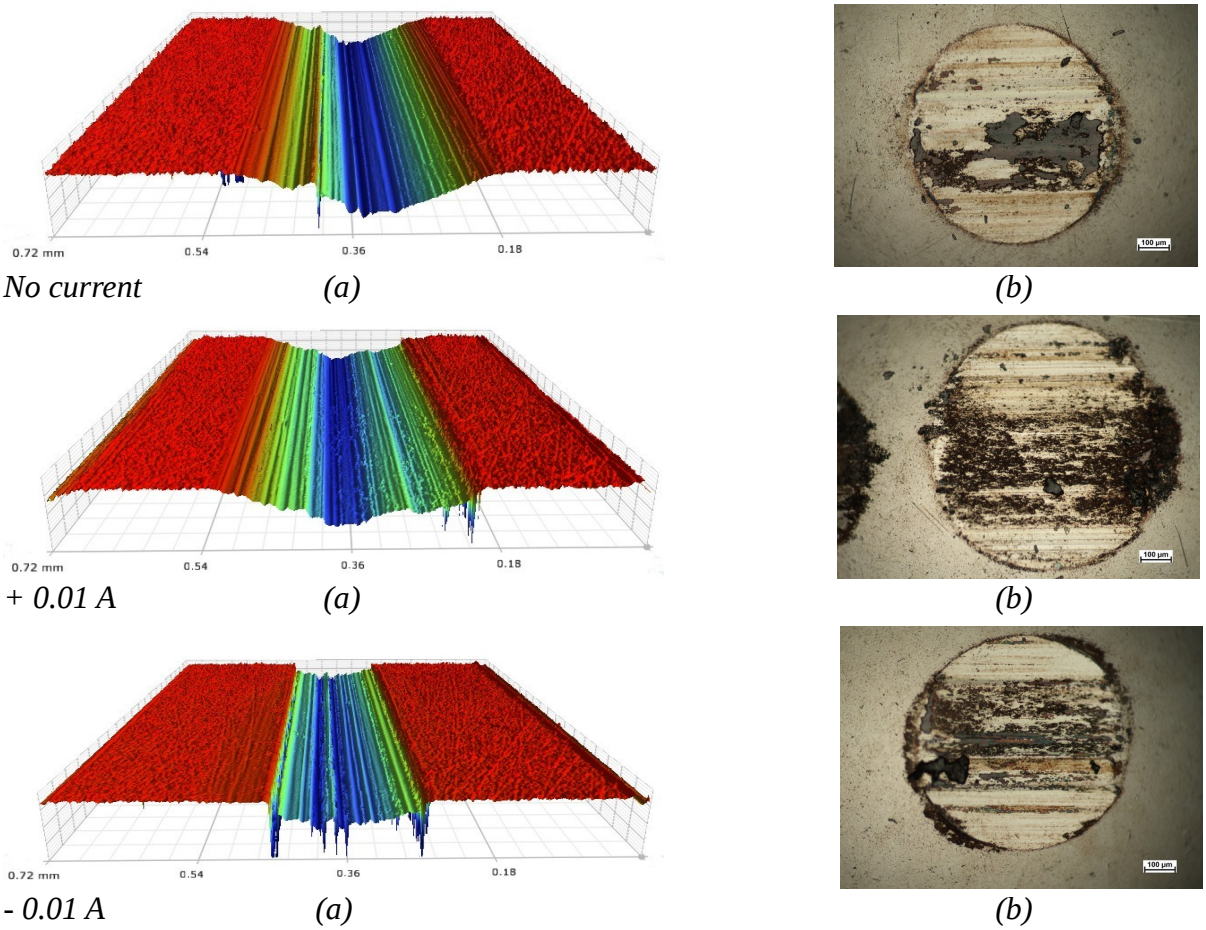

Figure 16: Analysis of Steel disc and Steel ball wear scars obtained under different current conditions using 3D microscope (a) to analyze disc wear scars and optical microscope (b) for the observation of the ball surface counterpart

4.2 Low Ti-DLC

4.2.1 Low Ti-DLC – Steel

Friction and Resistance Analysis

Friction and resistance data for Low Ti-DLC – Steel contact is presented in Figure 17. It can be seen that COF of Low Ti-DLC – Steel contact is quite constant, averaging around 0.2 for all electric current conditions. This was expected since DLC coatings are known for their low friction coefficient in dry sliding conditions. No specific influence of electric current on the COF of Low Ti-DLC – Steel contact was observed. Voltage drop data were collected during static and sliding conditions. A substantial increase in resistance was observed going from static to sliding conditions. Voltage drop measurements during sliding were between 0.6 V – 0.8 V for negative current and slightly higher, 0.8 – 1 V, when positive current was applied. The resistance of Low Ti-DLC – Steel contact was almost two times higher than that of Steel – Steel contact during sliding. Static voltage drop measurements immediately after sliding also show higher resistance for positive currents. After detaching and reattaching the sample to the same spot and subsequently on to a fresh surface, resistance dropped as expected.

Surface Analysis

Wear scars on the surface of both counterparts were analyzed using an optical microscope. The wear track profiles presented in Figure 18 correspond to the width and depth of the wear scar. First thing that can be observed from the wear scar profiles chart is that electric current has a relatively significant effect on the wear rate. Wear rate is the lowest when no current is applied. When negative current is present, the wear is slightly higher and is at its highest under positive current conditions. It could also be noted that the wear scar is slightly bigger when greater currents are applied. Some transfer of the DLC coating can be observed on the ball sample's worn surface in Figure 19, which is especially significant under positive current conditions.

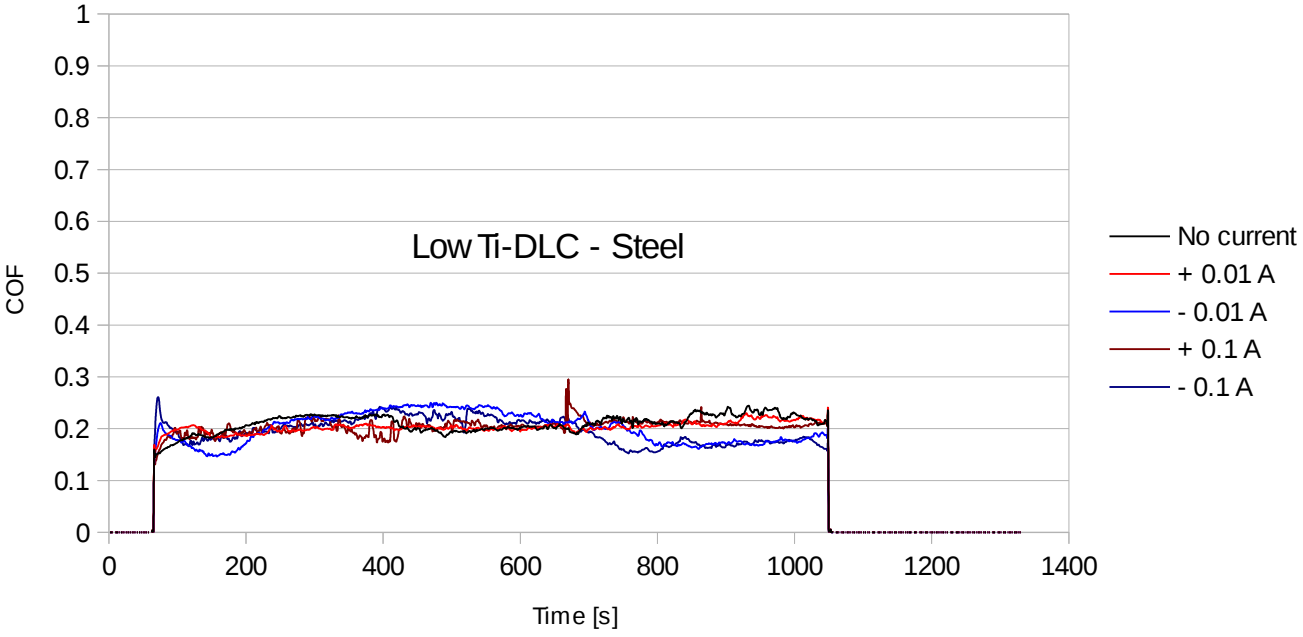

(a)

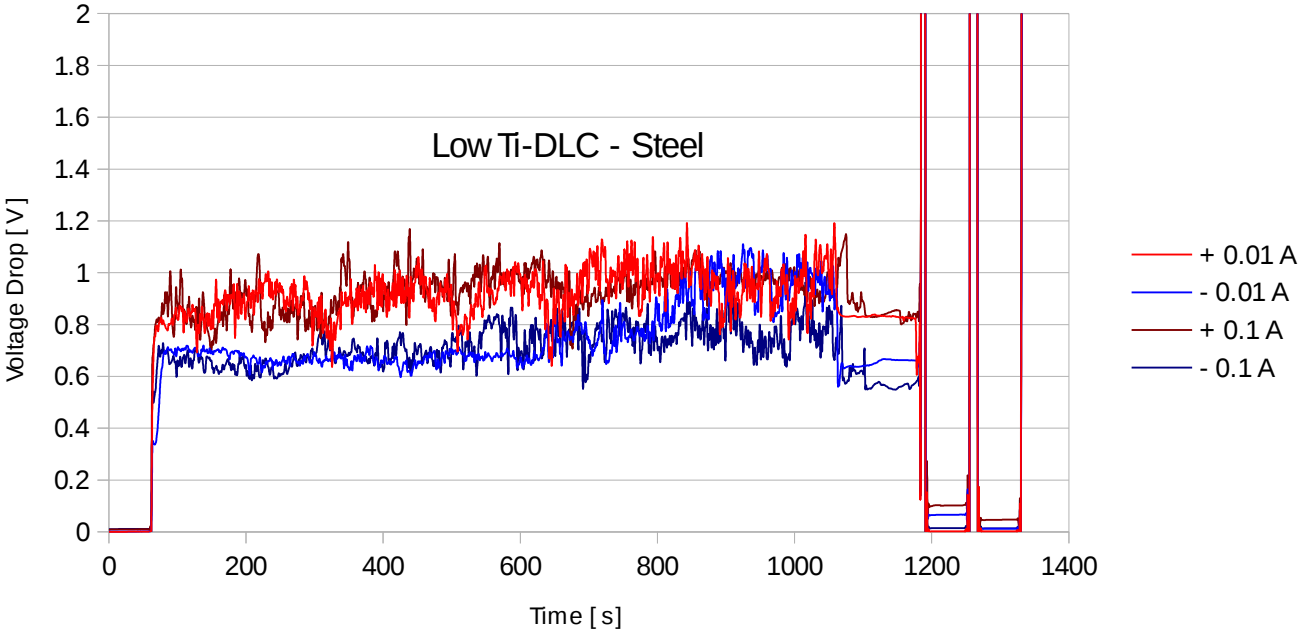

(b)

Figure 17: Coefficient of friction (a) and Voltage drop (b) of Low Ti-DLC – Steel contact

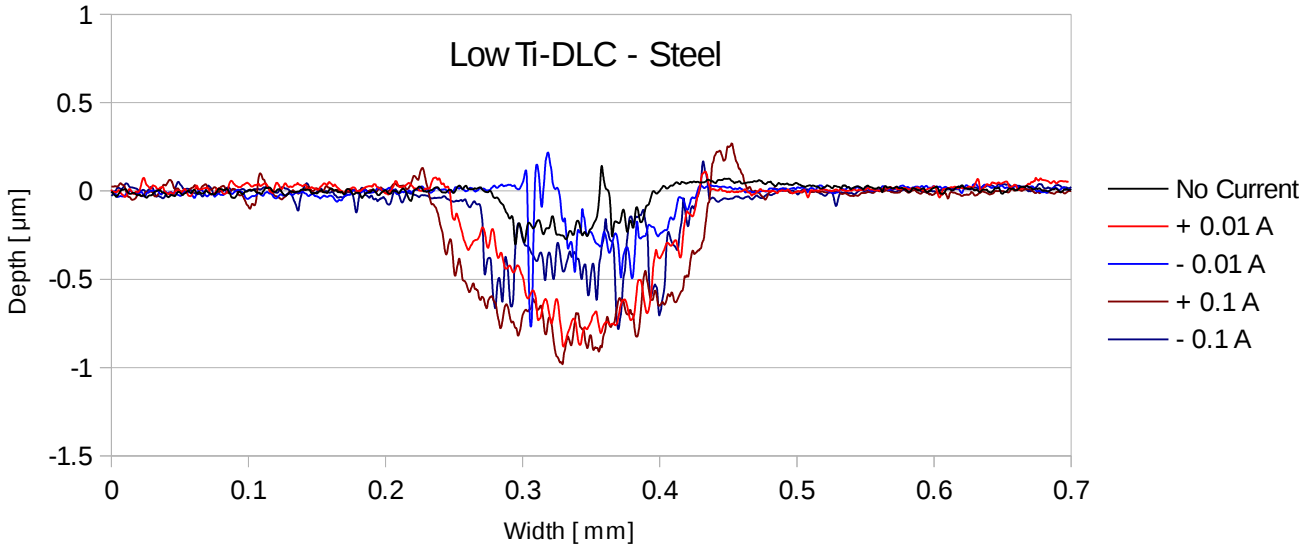

Figure 18: Wear scar profiles of Low Ti-DLC – Steel contact

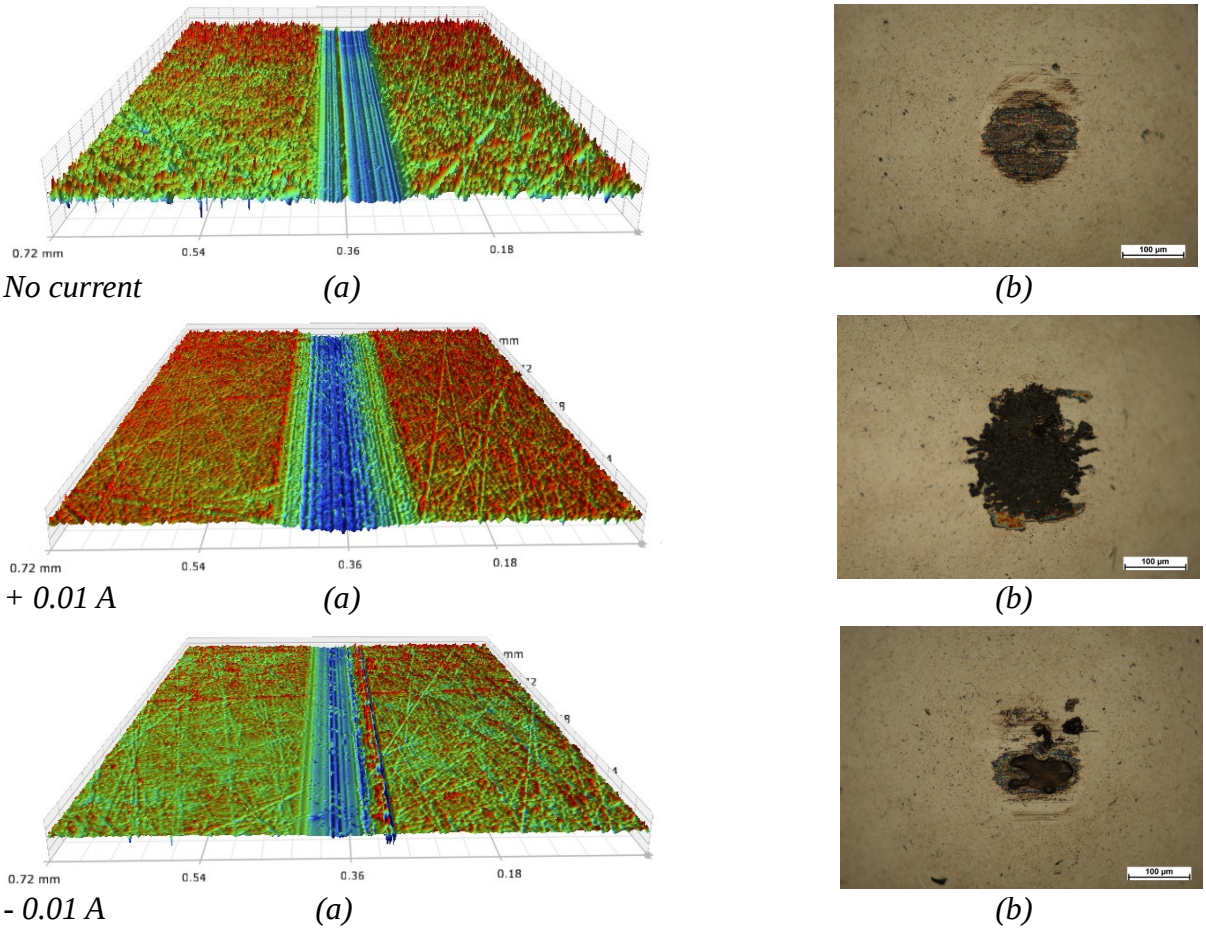

Figure 19: Analysis of Low Ti-DLC disc and Steel ball wear scars obtained under different current conditions using 3D microscope (a) to analyze disc wear scars and optical microscope (b) for the observation of the ball surface counterpart

4.2.2 Low Ti-DLC – Low Ti-DLC

Friction and Resistance Analysis

Friction and resistance data for Low Ti-DLC – Low Ti-DLC contact is presented in Figure 20. COF of the contact was again quite constant after a very short initial run-in period for all electric current conditions, except for a few spikes during both negative and positive 0.1 A current conditions. Friction spikes could be the result of wear debris of the coating getting stuck in the sliding contact as it can be seen from the pictures in Figure 22, some of the coating gets removed and some transferred to the ball surface counterpart. COF of friction was again quite low, around 0.2. The interesting thing was that COF of Low Ti-DLC – Low Ti-DLC contact, where both counterparts were coated, averaged around the same value as the COF of Low Ti-DLC – Steel contact where only the disc sample was coated. It did however show a decrease in resistance when both counterparts were coated, averaging between 0.4 – 0.5 V for all electric current conditions as it can be seen in Figure 20 (b). Some correlation between COF and voltage drop measurements was observed. For measurements with electric current of 0.1 A applied, it can be seen in Figure 20 that friction spikes correspond to the resistance drops in voltage drop measurements. The phenomena is not reversed because there were no friction spikes observed that would be in agreement with the resistance spikes. Therefore it could be said that COF has some influence on the electric resistance in the contact, but the resistance of the contact does not directly affect the COF. Voltage drop data were collected during static conditions as well. Static voltage drop measurements immediately after sliding again showed higher resistance for positive currents. After detaching and reattaching the sample to the same spot and subsequently to the fresh surface, resistance dropped as expected.

Surface Analysis

Wear scars on the surface of both counterparts were analyzed using an optical microscope. The wear track profiles presented in Figure 21 correspond to the width and depth of the wear scar. It can be observed in Figure 22, that the amount of electric current had a substantial effect on the wear rate. Wear rate was the lowest when no current was applied or there was a negative current of 0.01 A. Positive current of 0.01 A induced a larger wear scar with very noticeable tearing marks as it can be seen in Figure 22. Positive and negative currents of 0.1 A showed an even greater worn surface, with large tear lines, probably caused by higher current densities.

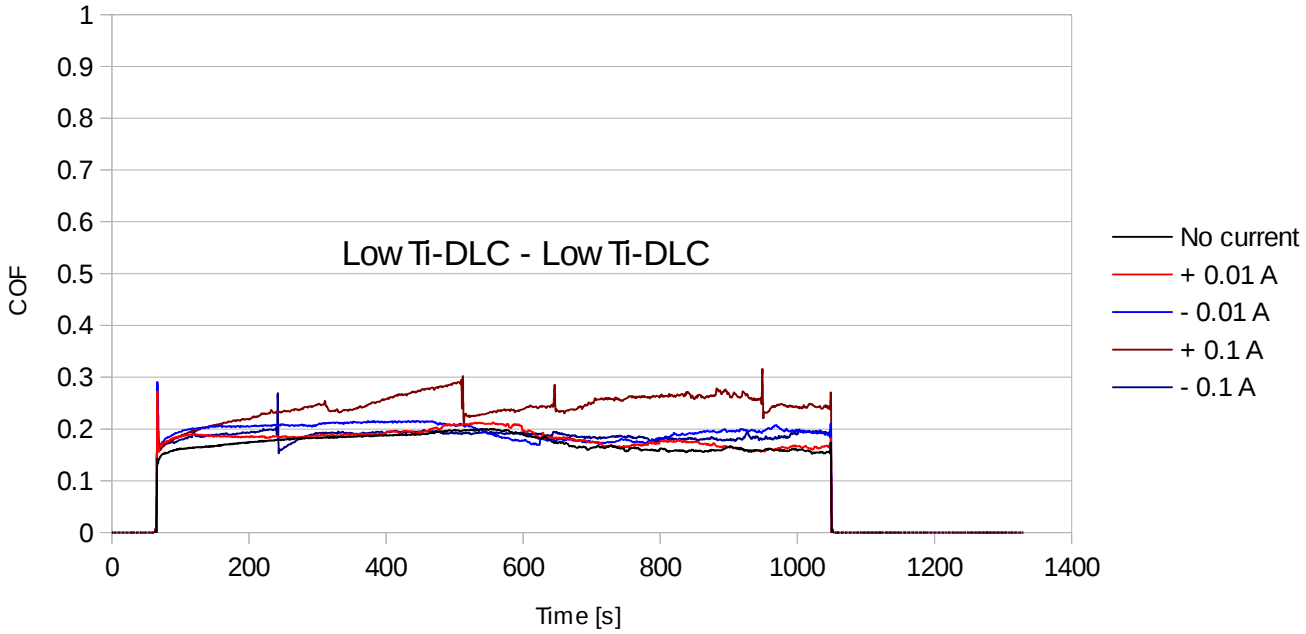

(a)

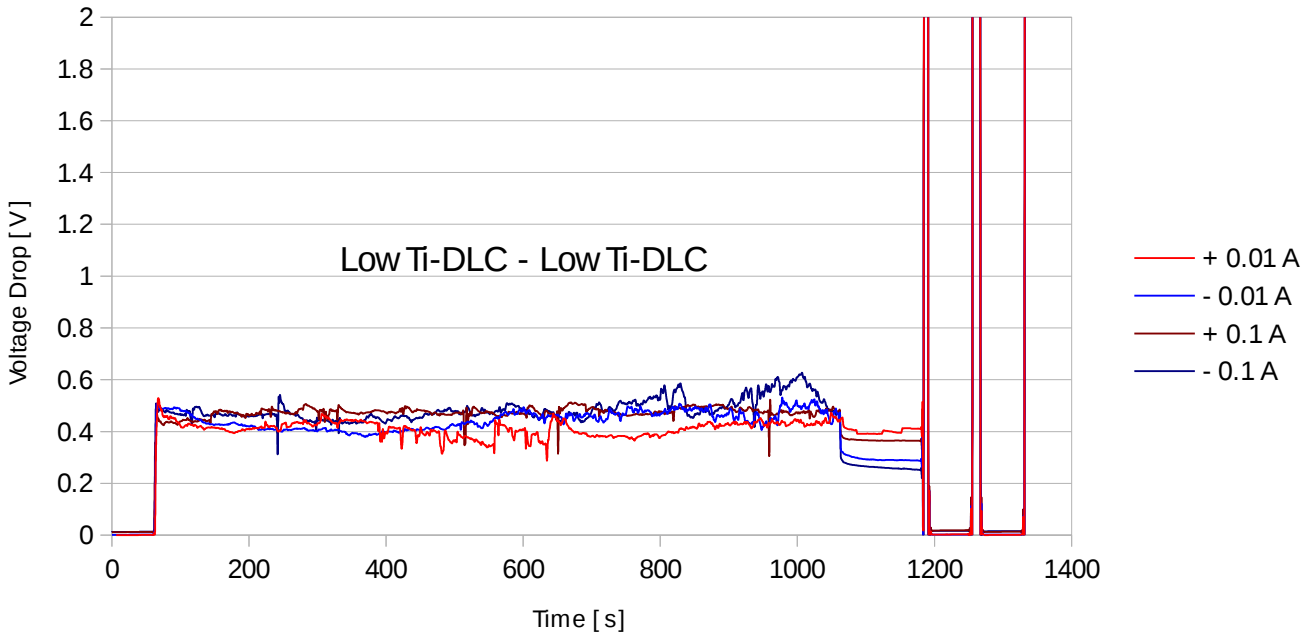

(b)

Figure 20: Coefficient of friction (a) and Voltage drop (b) of Low Ti-DLC – Low Ti-DLC contact

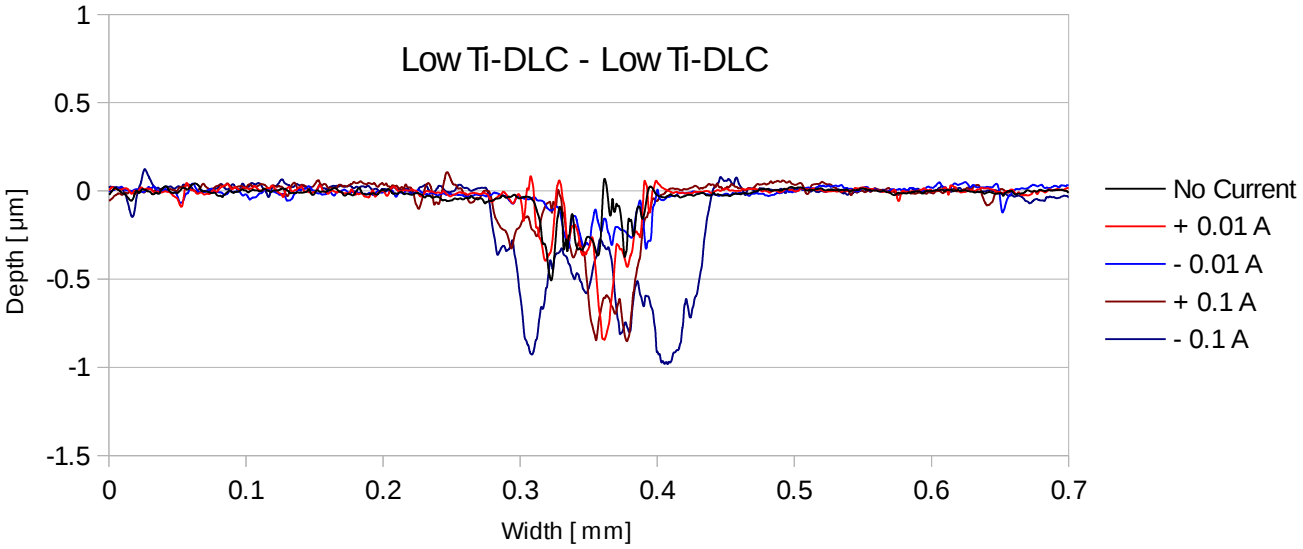

Figure 21: Wear scar profiles of Low Ti-DLC – Low Ti-DLC contact

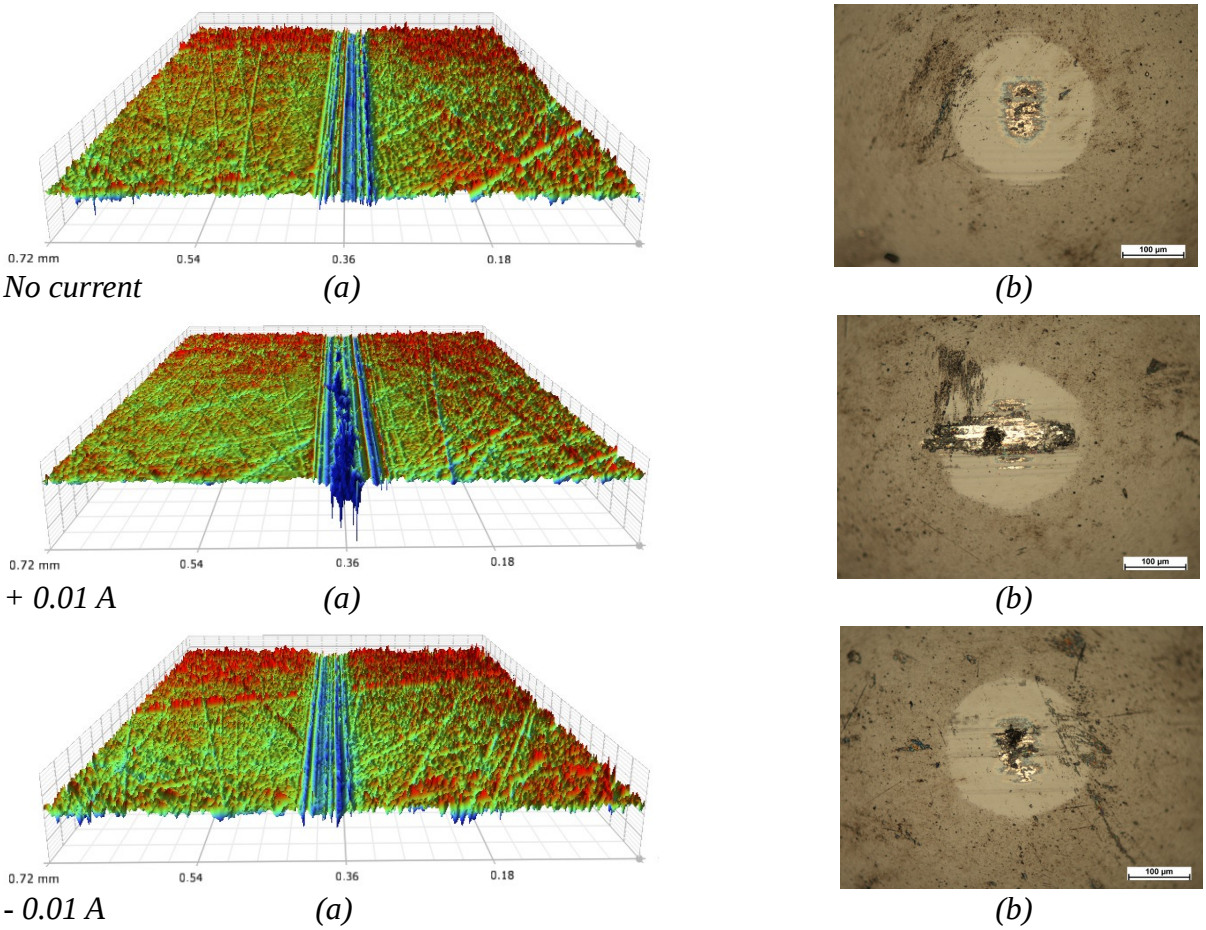

No current *(a)* *(b)*

+ 0.01 A *(a)* *(b)*

- 0.01 A *(a)* *(b)*

Figure 22: Analysis of Low Ti-DLC disc and Low Ti-DLC ball wear scars obtained under different current conditions using 3D microscope (a) to analyze disc wear scars and optical microscope (b) for the observation of the ball surface counterpart

4.3 High Ti-DLC

4.3.1 High Ti-DLC – Steel

Friction and Resistance Analysis

Friction and resistance data for High Ti-DLC – Steel contact is presented in Figure 23. High Ti-DLC – Steel contact had an average COF between 0.2 – 0.3. The COF was quite similar to the COF values obtained for Low Ti-DLC – Steel contact. After the run-in period, the COF dropped to around 0.2 for all measurements and was steadily increasing over the course of the whole test. The increase of COF was minor for all test conditions except for when positive electric current of 0.1 A was applied. It can be seen in Figure 23 (a), how COF around 700 second into the test, abruptly increased and finished of at the end of the test at more than double the value of the initial COF. The test with positive electric current of 0.1 A applied, was repeated four times in total, to ensure no environmental influence could effect the measurement. All of the tests yielded the same result. Voltage drop data were collected during static and sliding conditions. It can be observed from the voltage drop measurements displayed in Figure 23 (b), that the resistance is higher when positive current is applied, ranging around 0.6 V at 0.01 A and 0.8 V at 0.1 A. Correlation between the COF and resistance can be observed for the positive electric current of 0.1 A at 700 second into the test, where there is gradual drop in resistance. It can be said that the resistance drop is analogous to the increase of COF at 700 second mark. Both negative currents, 0.01 A and 0.1 A, average around 0.4 V. Static voltage drop measurements right after sliding follow a similar pattern. Last two static voltage drop measuring steps exhibited a drop in resistance for all current conditions as already seen in previous cases.

Surface Analysis

Wear scars on the surface of both counterparts were analyzed using an optical microscope. The wear track profiles presented in Figure 24 correspond to the width and depth of the wear scar. The wear profiles for High Ti-DLC – Steel contact in Figure 24 and images of the wear tracks in Figure 25 exhibit wider and shallower wear scars than the ones previously observed for other material combinations. Width of the scars averaged around 0.3 mm while the depth was around 0.5 μm. Wear scar profiles show a similar pattern for all electric current conditions therefore it could be said that there is no noticeable correlation between the electric current and the wear rate of the samples.

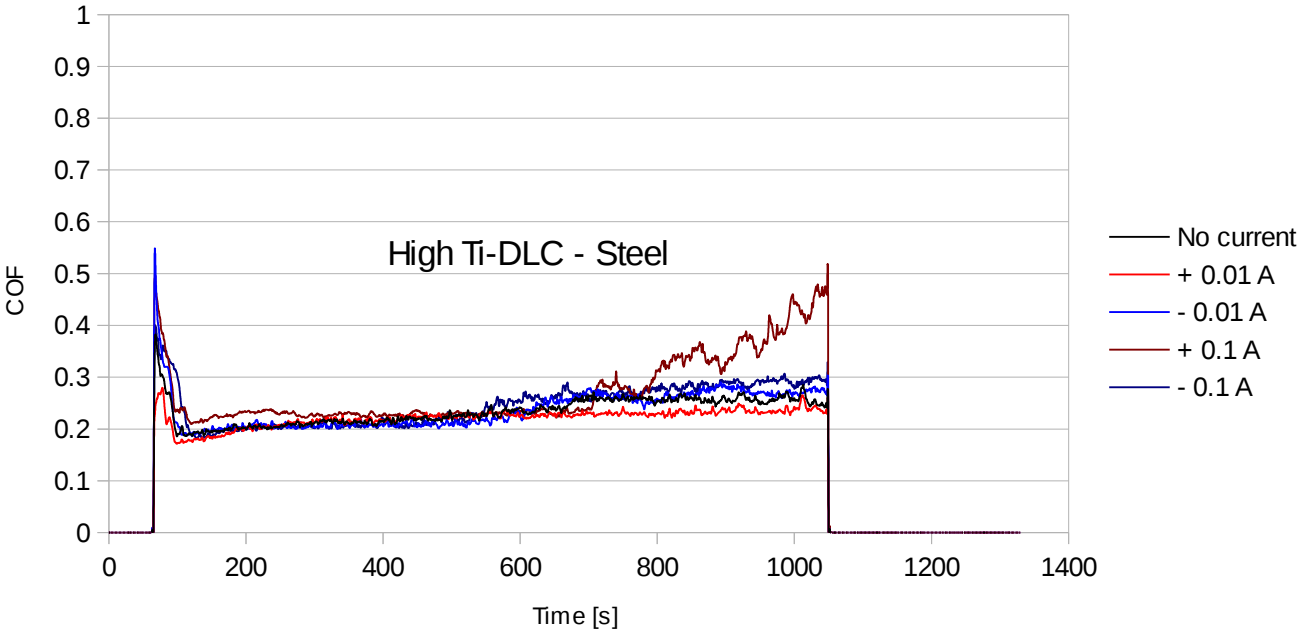

(a)

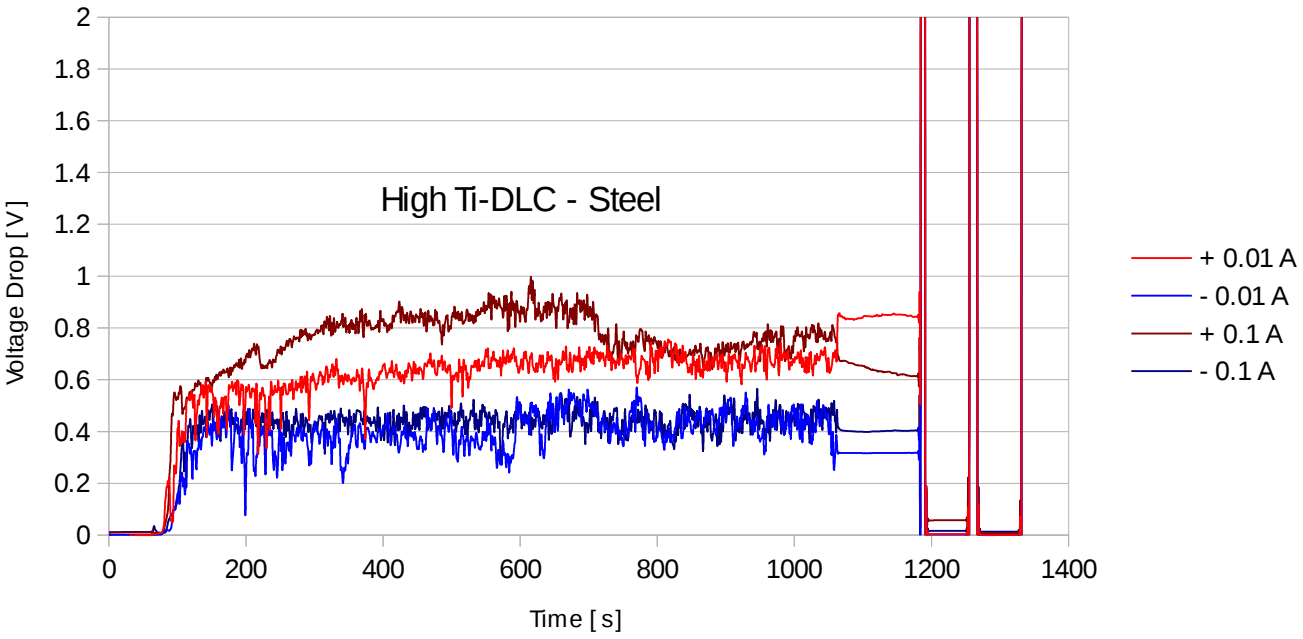

(b)

Figure 23: Coefficient of friction (a) and Voltage drop (b) of High Ti-DLC – Steel contact

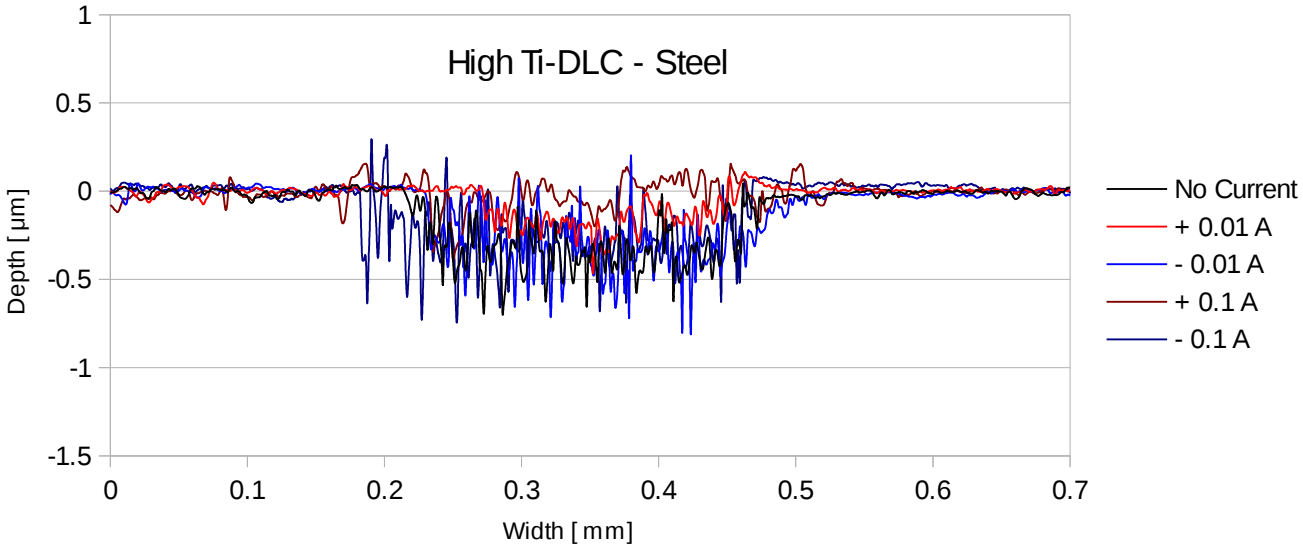

Figure 24: Wear scar profiles of High Ti-DLC – Steel contact

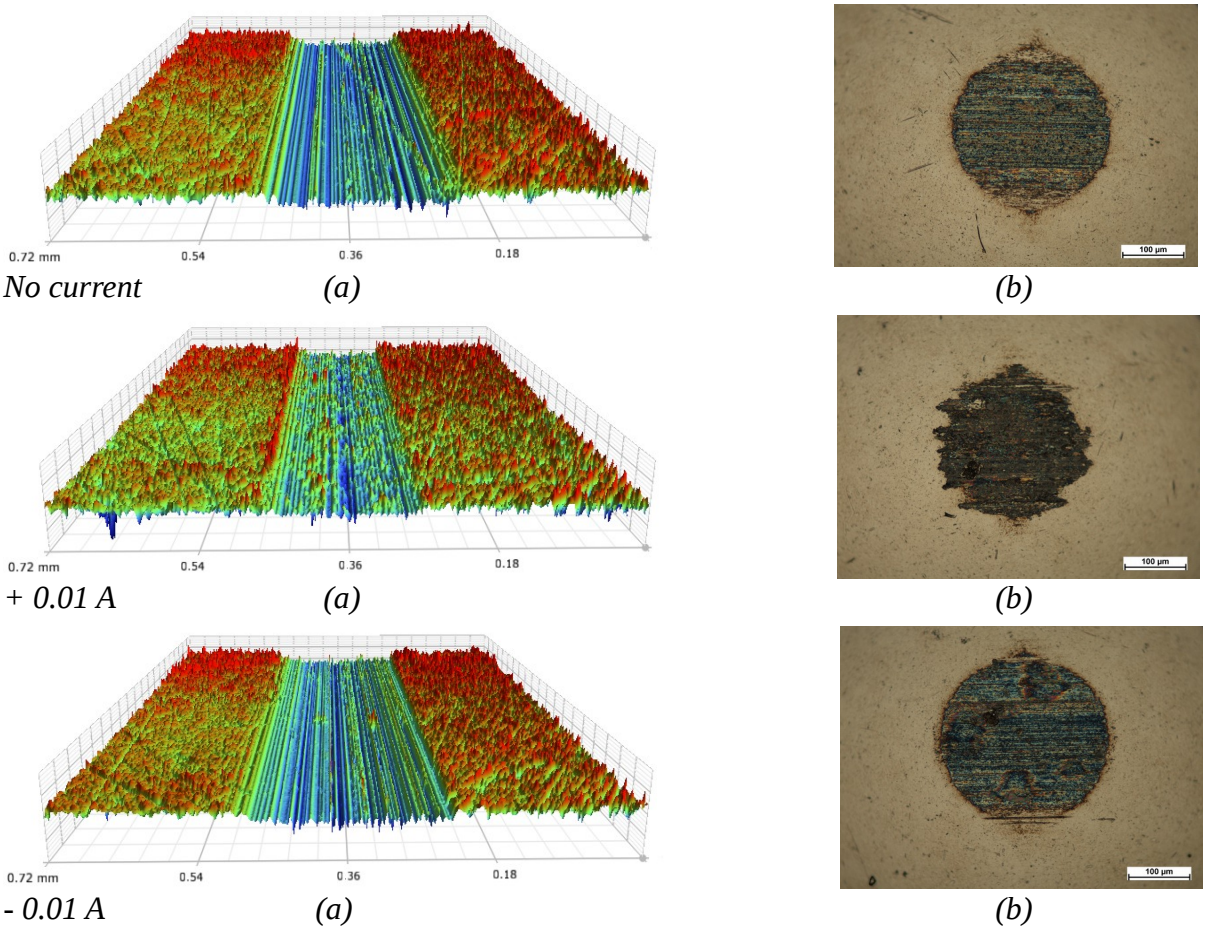

No current *(a)* *(b)*

+ 0.01 A *(a)* *(b)*

- 0.01 A *(a)* *(b)*

Figure 25: Analysis of High Ti-DLC disc and Steel ball wear scars obtained under different current conditions using 3D microscope (a) to analyze disc wear scars and optical microscope (b) for the observation of the ball surface counterpart

4.3.2 High Ti-DLC – High Ti-DLC

Friction and Resistance Analysis

Friction and resistance data for High Ti-DLC – High Ti-DLC contact is presented in Figure 26. Friction coefficient for High Ti-DLC – High Ti-DLC contact was very steady, averaging around 0.2 for all electric current conditions. There was almost no run-in period, the COF rose to the value of 0.2 and remained there with minor increase for when there was no current or positive current was applied. Voltage drop data were collected during static and sliding conditions. In the case of High Ti-DLC – High Ti-DLC contact, a difference can be observed in Figure 26 (b) between when 0.01 A and 0.1 A electric current is applied. For the first 400 seconds of testing, 0.01 A electric current measurements averaged below 0.2 V, while the 0.1 A electric current measurements ranged between 0.3 – 0.4 V. 400 seconds into the test, resistance of the 0.01 A positive electric current conditions increased to 0.4 V, showing similar behavior to the measurements at 0.1 A applied electric current. Measurements at 0.01 A positive electric current conditions were repeated three times, to discard any external influence. The extra measurements produced similar results. Static voltage drop measurements showed a similar pattern as in sliding conditions, producing higher resistance for 0.1 A electric currents and lower for 0.01 A electric current conditions. High drops in resistance can be observed for the detaching and reattaching of the samples to the same spot following by reattaching on to a fresh surface.

Surface Analysis

Wear scars on the surface of both counterparts were analyzed using an optical microscope. The wear track profiles presented in Figure 27 correspond to the width and depth of the wear scar. Wear profiles presented in Figure 27 and images of wear scars in Figure 28 show an interesting wear behavior of High Ti-DLC – High Ti-DLC contact. Wear scar profile with no electric current conditions shows larger wear rate than the ones where electric current was applied. No other correlation between the wear rate and different electric current conditions was observed.

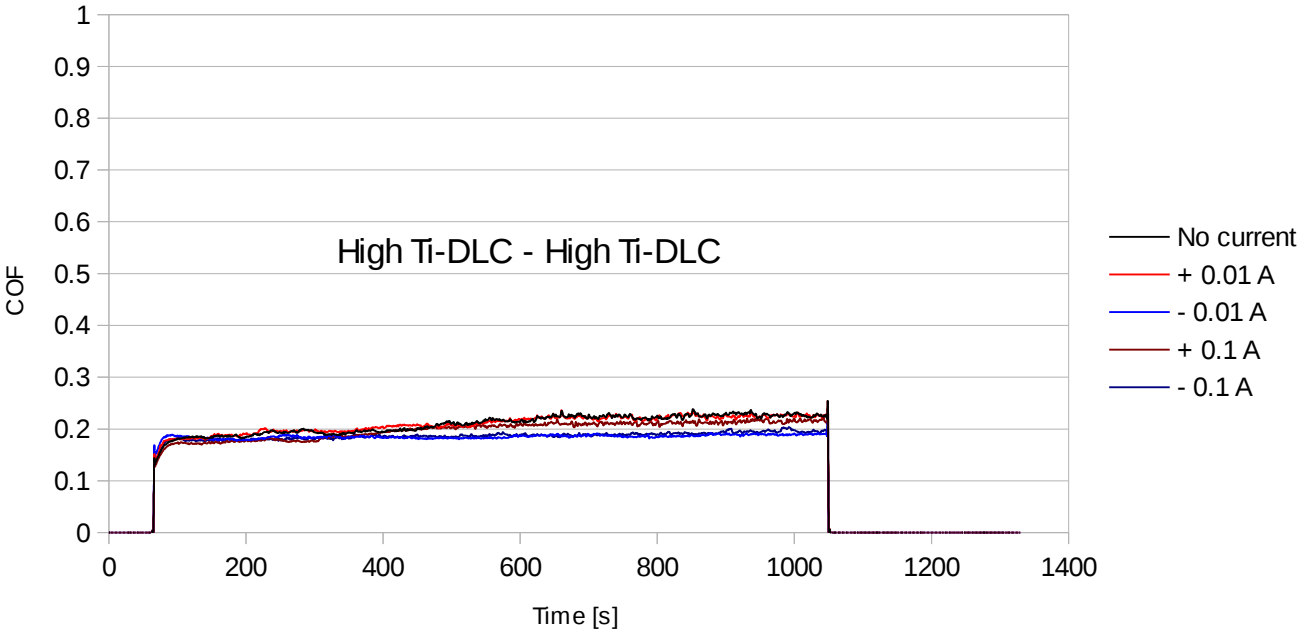

(a)

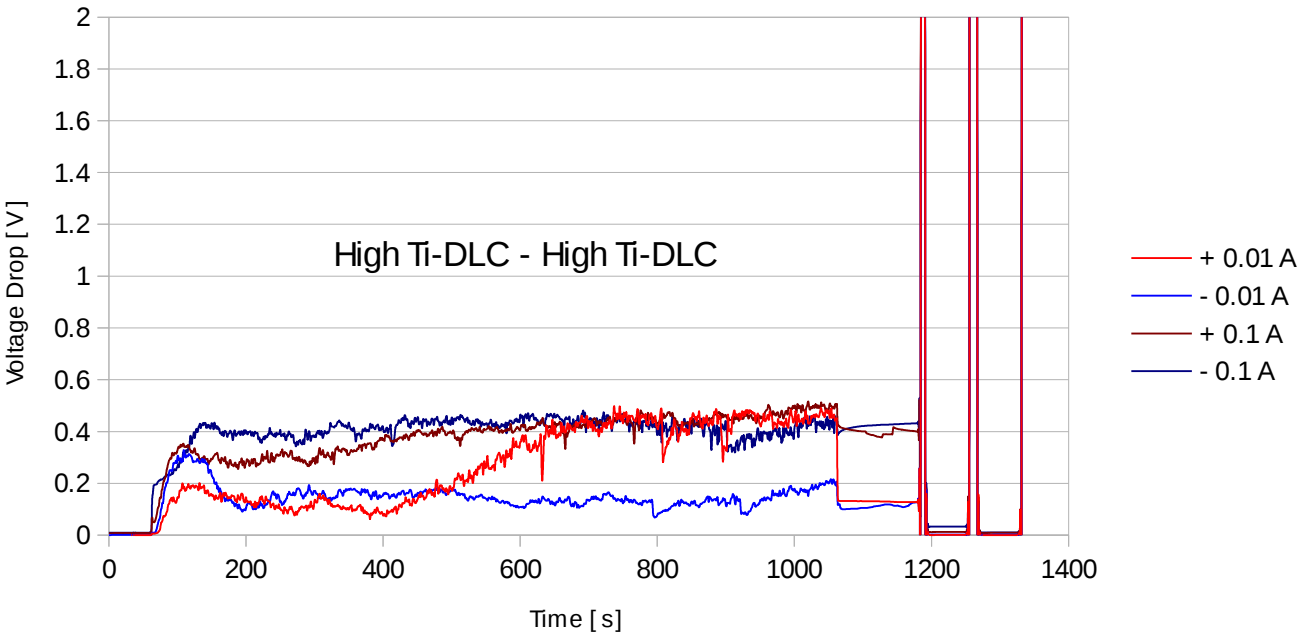

(b)

Figure 26: Coefficient of friction (a) and Voltage drop (b) of High Ti-DLC – High Ti-DLC contact

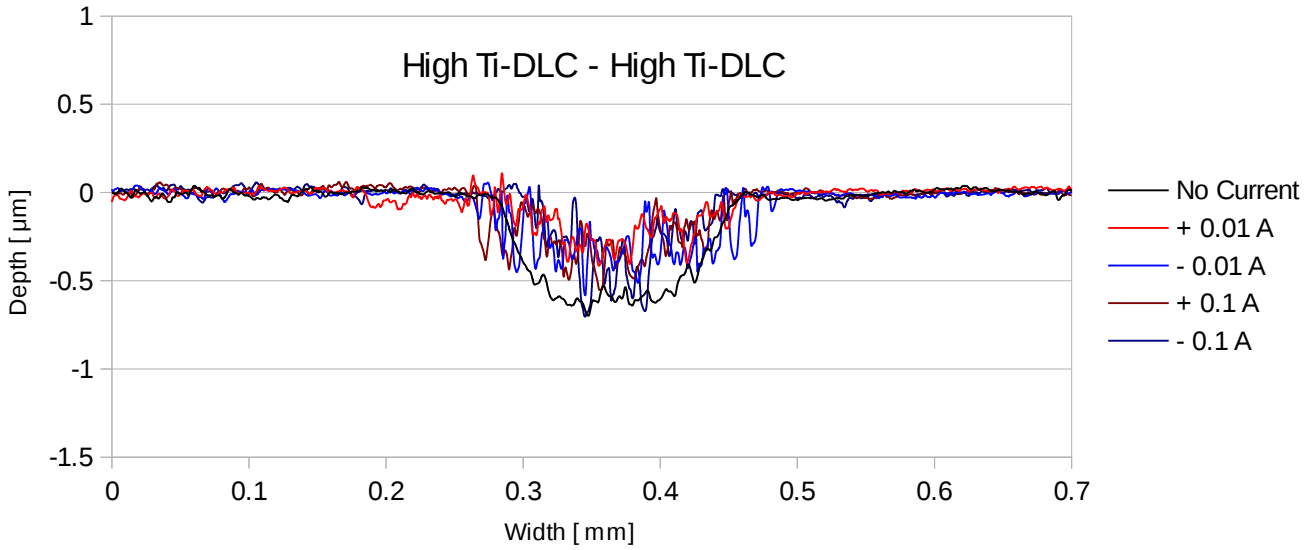

Figure 27: Wear scar profiles of High Ti-DLC – High Ti-DLC contact

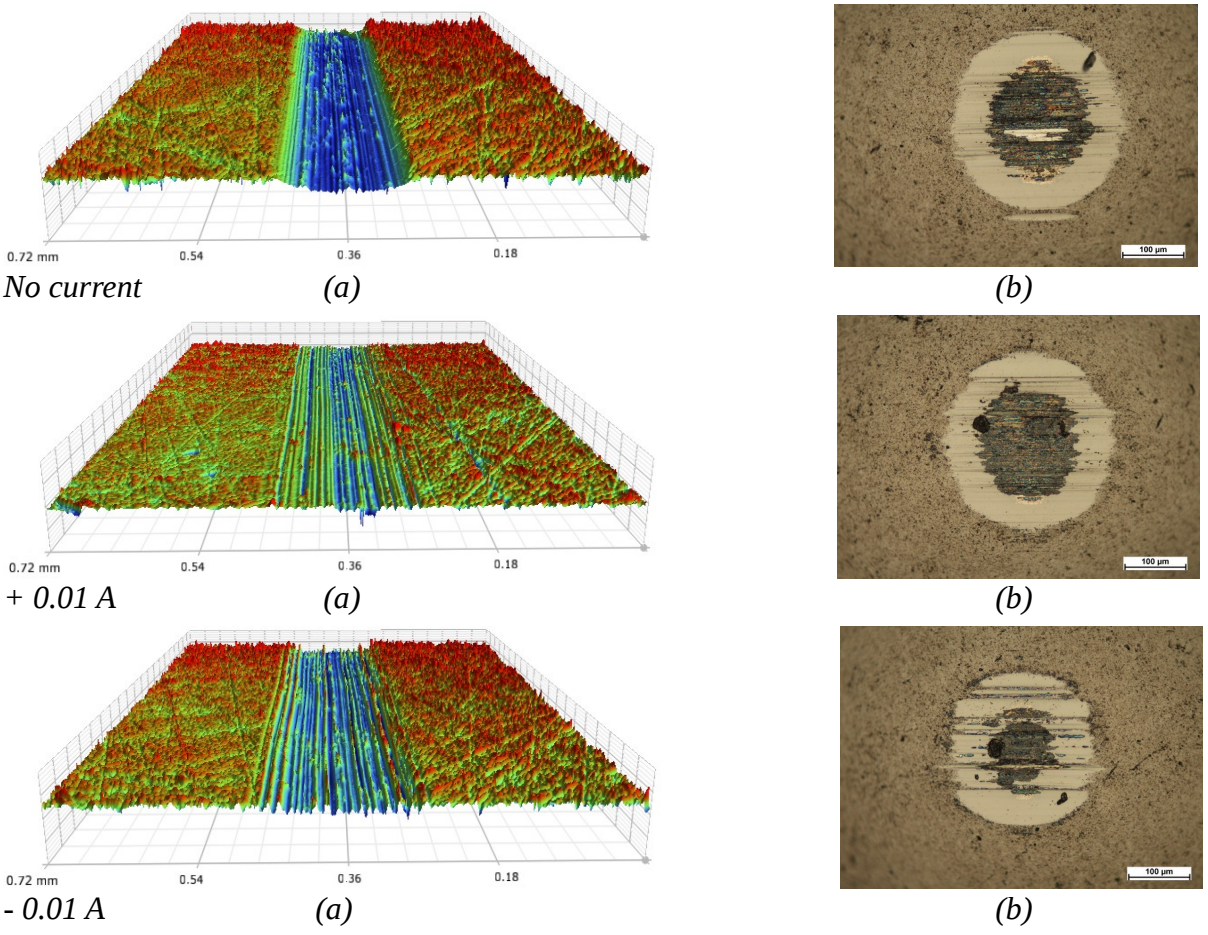

Figure 28: Analysis of High Ti-DLC disc and High Ti-DLC ball wear scars obtained under different current conditions using 3D microscope (a) to analyze disc wear scars and optical microscope (b) for the observation of the ball surface counterpart

4.4 Low W-DLC

4.4.1 Low W-DLC – Steel

Friction and Resistance Analysis

Friction and resistance data for Low W-DLC – Steel contact is presented in Figure 29. The COF of Low W-DLC – Steel contact appears to be low for all current conditions, particularly when there is no electric current or there is positive current applied. COF averaged slightly below 0.2 for no current and positive current conditions. For negative electric currents applied, the friction coefficient ranged between 0.2 – 0.3. It could be said that there is a reversed phenomena compared to Ti-DLC coatings. Higher friction coefficients were usually observed for positive current, while in Low W-DLC – Steel contacts, negative currents displayed higher friction values. Voltage drop data were collected during static and sliding conditions. The resistance of Low W-DLC – Steel contact, presented in Figure 29 (b), was somewhat unstable. Voltage drop measurements spanned from 0.4 V up to 1.2 V. Varying and relatively high resistance, as displayed in Figure 29 (b), does not show promise for electrical applications, where constant steady conduction is presumed. No distinct correlation could be drawn between the COF and voltage drop measurements for Low W-DLC – Steel contact. Static voltage drop measurements immediately after sliding showed lower resistance for 0.01 A electric current conditions. A large drop of almost 50 % can be observed for measurements at 0.01 A electric current applied (from 0.9 V to 0.5 V). After detaching and rejoining the samples, resistance drops can be observed for both steps, same spot and new spot respectively.

Surface Analysis

Wear scars on the surface of both counterparts were analyzed using an optical microscope. The wear track profiles presented in Figure 30 correspond to the width and depth of the wear scar. In general, there was little wear observed in the Low W-DLC – Steel contact for all test conditions, except for a few deep cuts at 0.1 A electric current conditions. The deep tears were probably the result of high current densities present in the contact, when the tearing of the coating occurred. Although the wear tears appear quite deep, no puncture of coating occurred. By observing wear profiles in Figure 30 and wear scar images in Figure 31, it could be said that positive currents produced larger wear scars, opposed to negative currents, where the wear scars appear to be smaller.

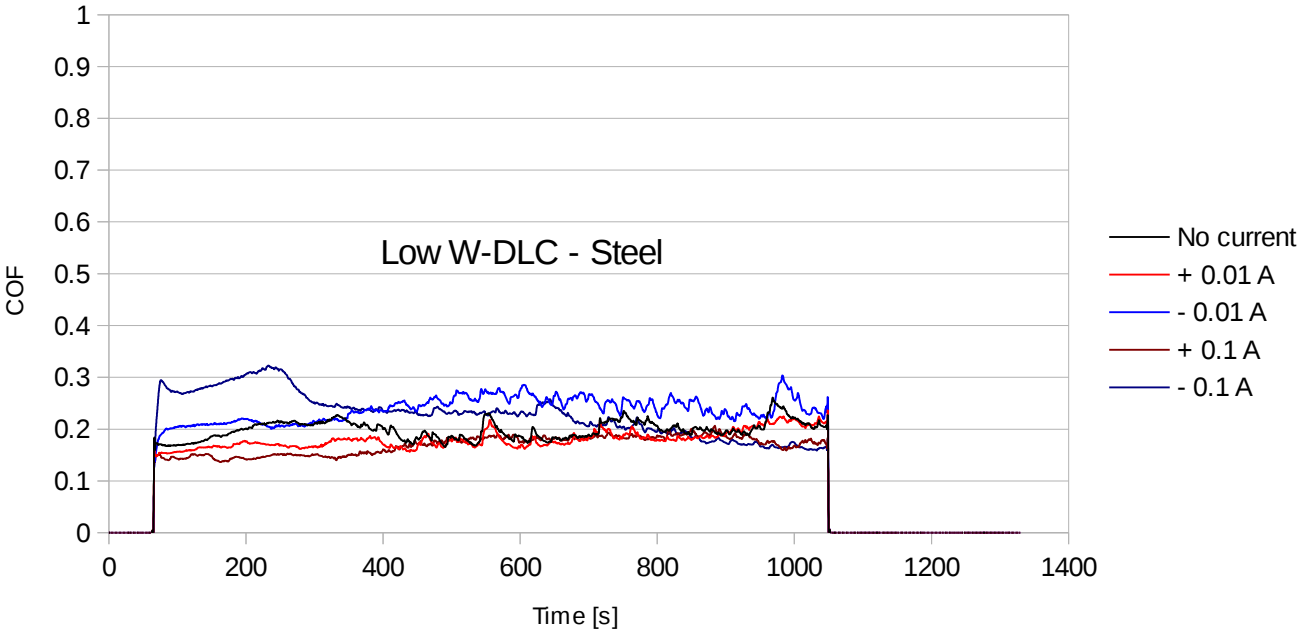

(a)

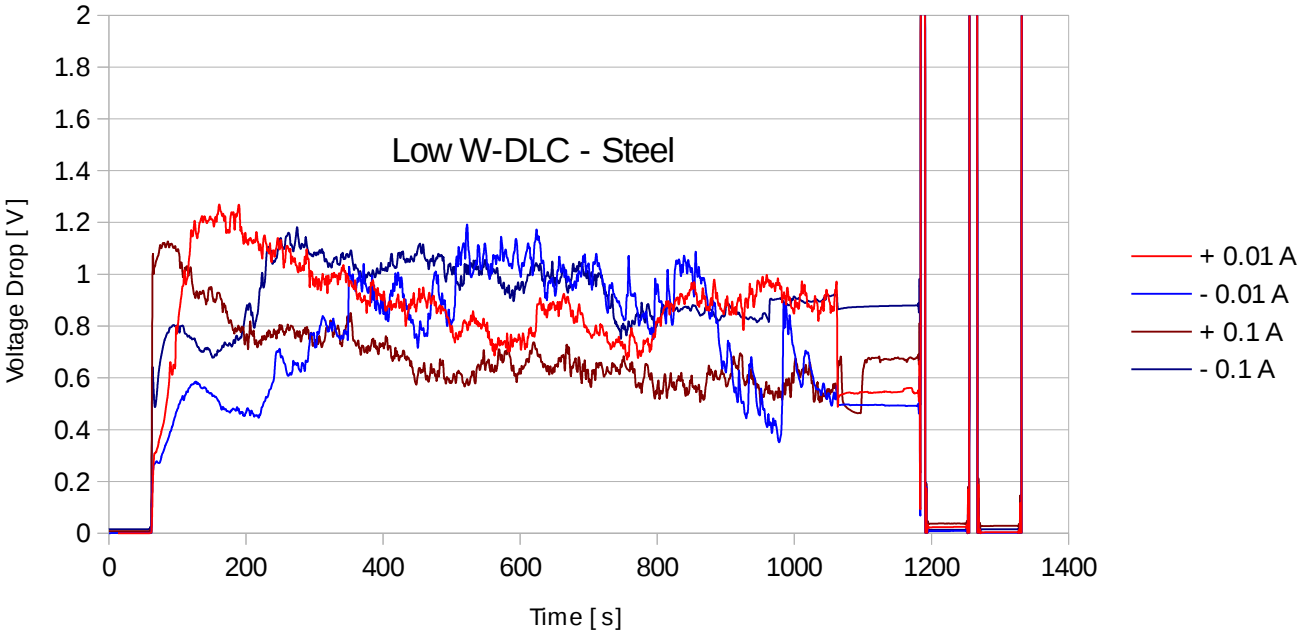

(b)

Figure 29: Coefficient of friction (a) and Voltage drop (b) of Low W-DLC – Steel contact

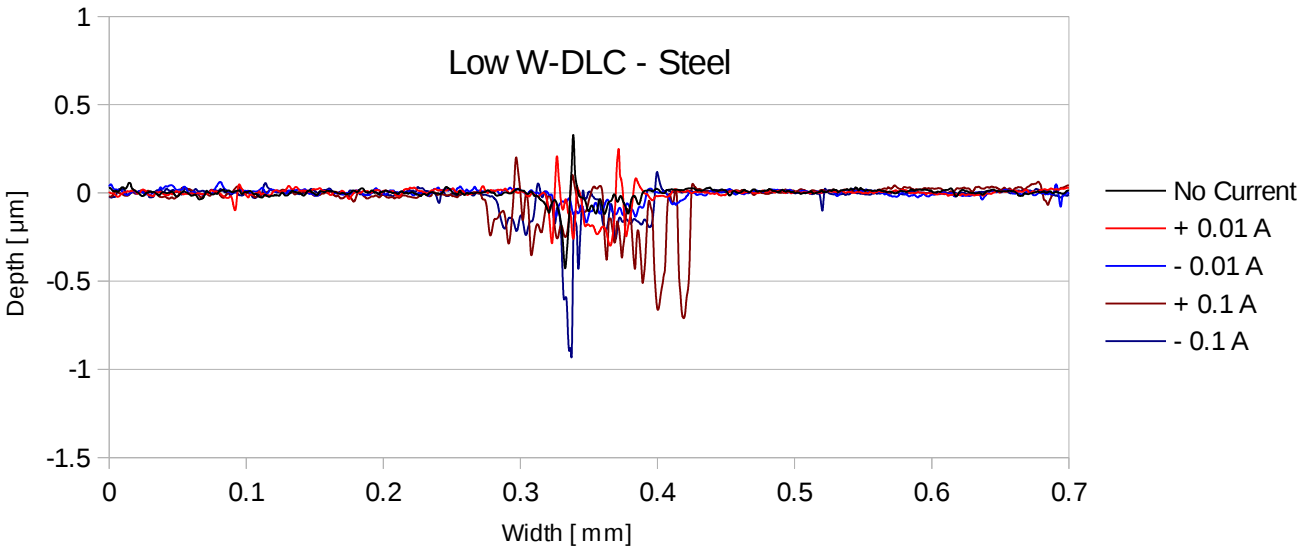

Figure 30: Wear scar profiles of Low W-DLC – Steel contact

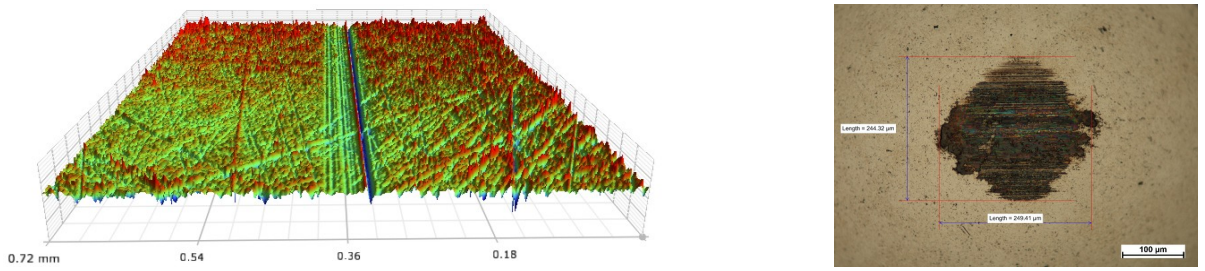

No current *(a)* *(b)*

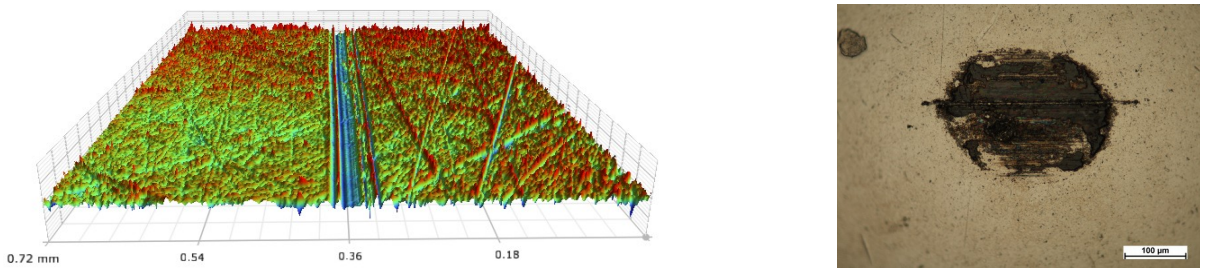

+ 0.01 A *(a)* *(b)*

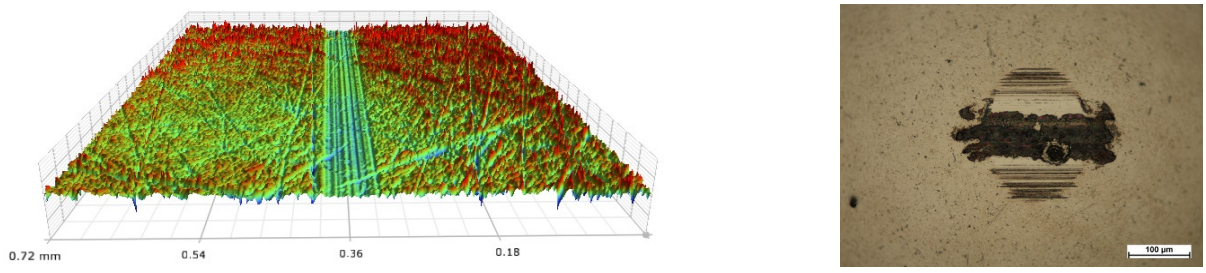

- 0.01 A *(a)* *(b)*

Figure 31: Analysis of Low W-DLC disc and Steel ball wear scars obtained under different current conditions using 3D microscope (a) to analyze disc wear scars and optical microscope (b) for the observation of the ball surface counterpart

4.5 High W-DLC

4.5.1 High W-DLC – Steel

Friction and Resistance Analysis

Friction and resistance data for High W-DLC – Steel contact is presented in Figure 32. High W-DLC – Steel contact friction coefficient ranged between 0.2 – 0.3 for all electric current conditions. The COF presented in Figure 32 (a) showed rather unstable behavior, especially in the second half of the test, where friction spikes can be observed in almost every test. The lowest and most stable friction coefficients were observed for tests at electric current of 0.1 A. Voltage drop measurements were done during static and sliding conditions and displayed in Figure 32 (b). The resistance of High W-DLC – Steel contact stabilized after a slightly longer run-in period of 300 seconds. Voltage drop measurements ranged from 0.4 V for negative currents to 0.6 V for positive currents. As in COF measurements, some erratic behavior can be observed in the second part of the testing for all test conditions. Tests conducted at negative electric current condition of 0.01 A displayed the most unstable behavior with relatively large spikes and drop in resistance. Static voltage drop data collected after sliding showed higher resistance for positive electric current conditions. After detaching and reattaching the sample to the same spot and subsequently on to a fresh surface, resistance dropped as in previous cases.

Surface Analysis

Wear scars on the surface of both counterparts were analyzed using an optical microscope. The wear track profiles presented in Figure 33 correspond to the width and depth of the wear scar. Wear profiles of High W-DLC – Steel contact in Figure 33 combined with images in Figure 34 revealed that very small amount of wear occurred in all electric current conditions. No deep tearing was detected that could have materialized due to high current densities. Slightly deeper wear scars on the disc sample were detected for positive current, which could correlate to higher resistance of positive currents in voltage drop measurements.

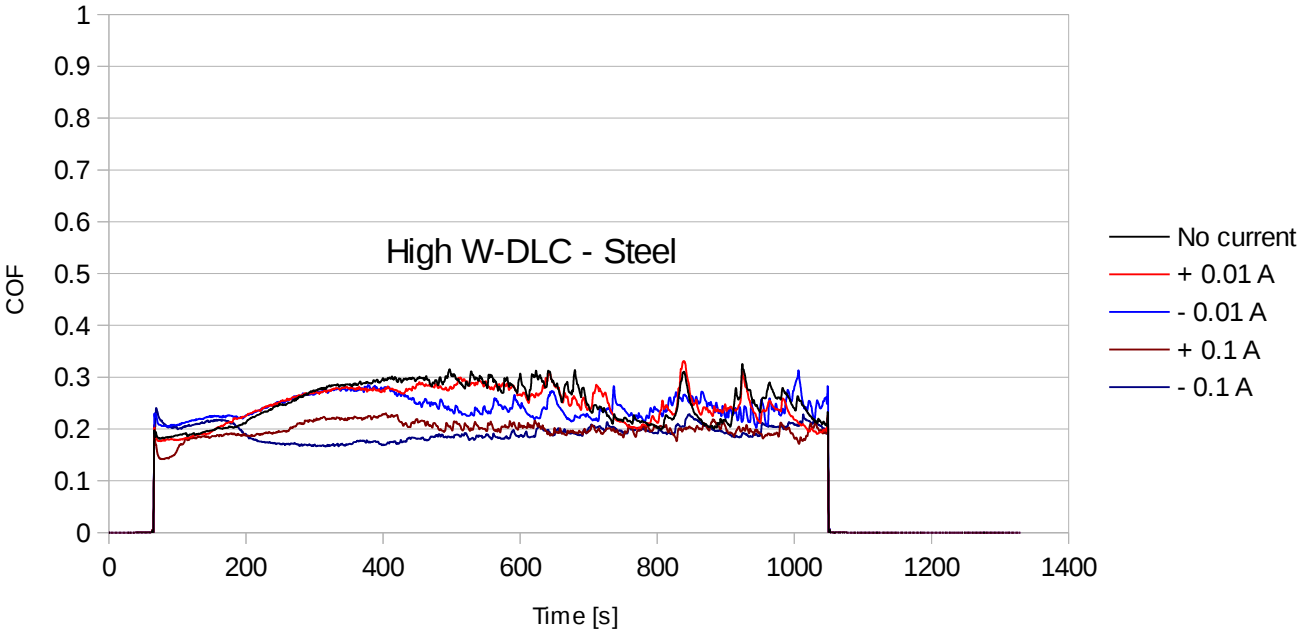

(a)

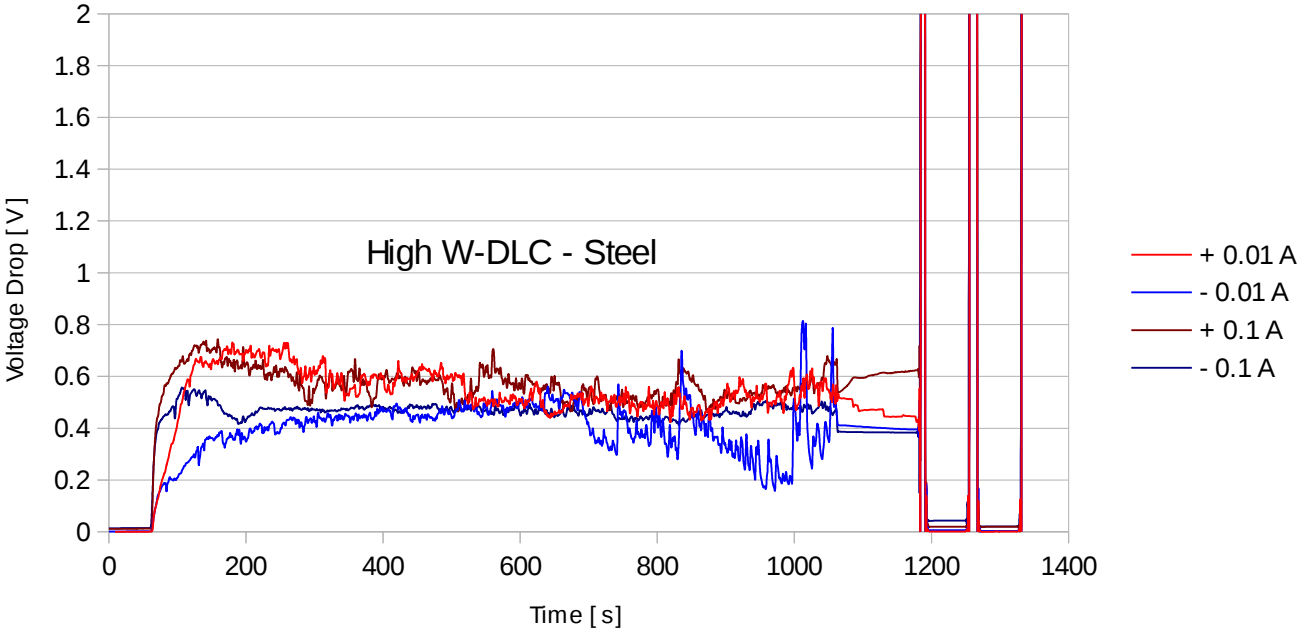

(b)

Figure 32: Coefficient of friction (a) and Voltage drop (b) of High W-DLC – Steel contact

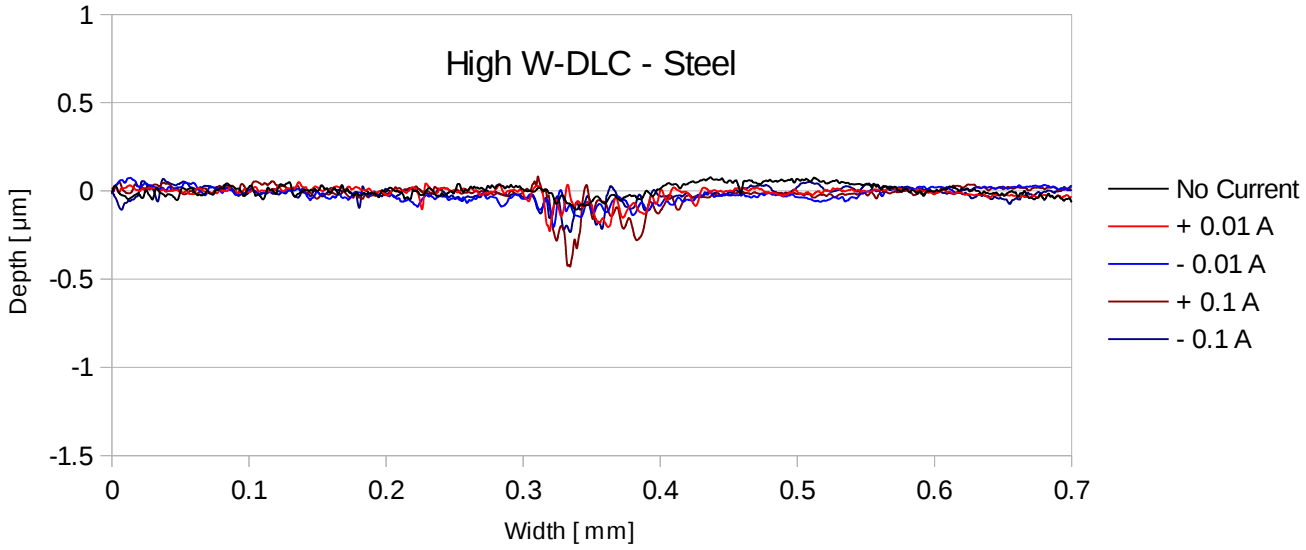

Figure 33: Wear scar profiles of High W-DLC – Steel contact

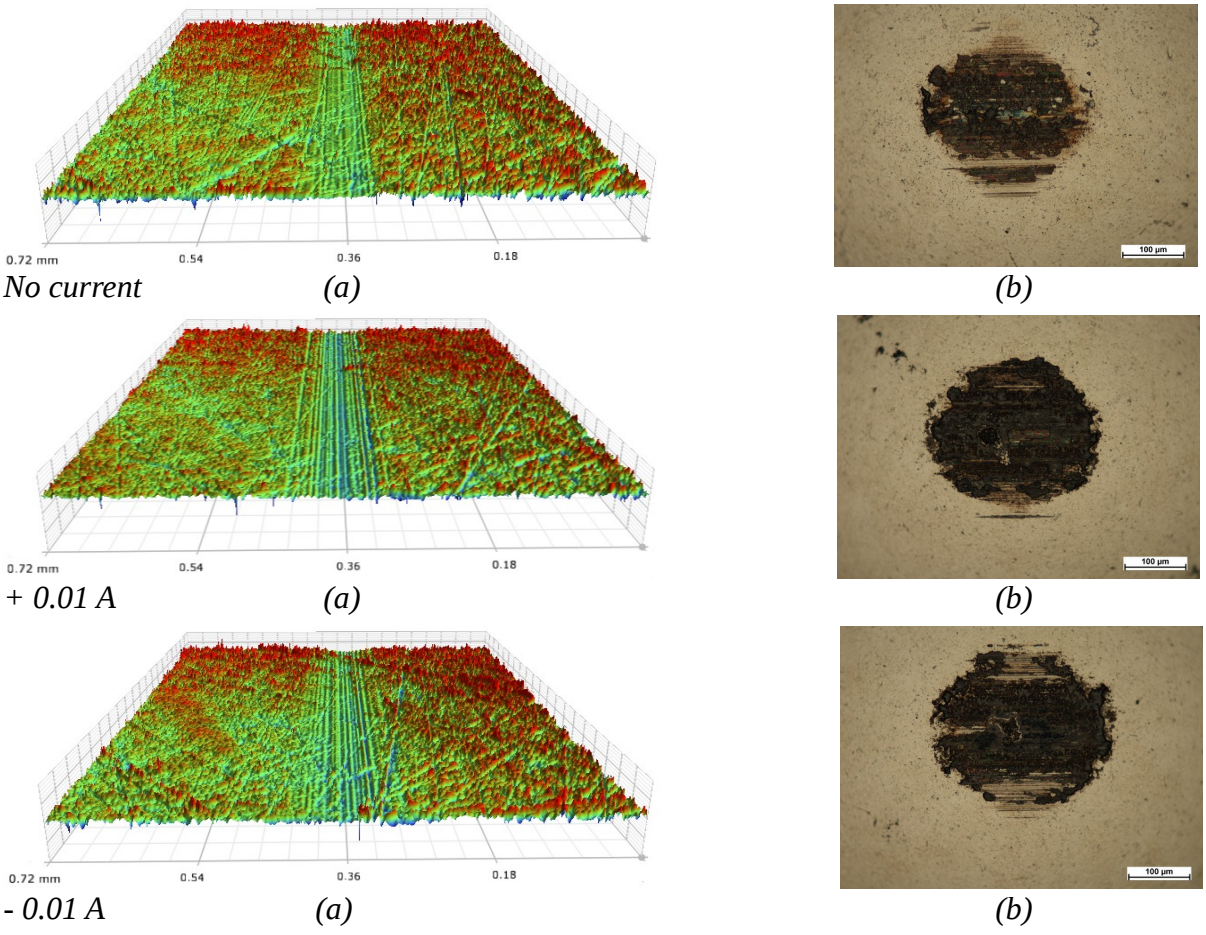

No current *(a)* *(b)*

+ 0.01 A *(a)* *(b)*

- 0.01 A *(a)* *(b)*

Figure 34: Analysis of High W-DLC disc and Steel ball wear scars obtained under different current conditions using 3D microscope (a) to analyze disc wear scars and optical microscope (b) for the observation of the ball surface counterpart

4.5.2 High W-DLC – High W-DLC

Friction and Resistance Analysis

Friction and resistance data for High W-DLC – High W-DLC contact is presented in Figure 35. COF for High W-DLC – High W-DLC contact ranged between 0.1 – 0.2. Friction curves display very low and stable friction coefficients for all test conditions. An interesting observation can be made from Figure 35 (a), that friction coefficients where electric current was applied are lower than when there was no current present. Voltage drop measurements were done during static and sliding conditions and displayed in Figure 35 (b). The resistance of High W-DLC – High W-DLC contact was very stable for all test conditions after the initial run-period during the first 200 seconds. However there was quite a difference in resistance between different electric current conditions. Both negative current conditions of 0.01 A and 0.1 A displayed higher resistance than their positive counterparts. Voltage drop measurements for negative electric current conditions were around 0.3 V. Voltage drop measurements for positive electric current at 0.1 A was around 0.1 V and continued to decrease, while at 0.01 A, voltage drop measurements averaged below 0.1 V and towards the end of the test reached resistance values of static contacts. Static voltage drop measurements obtained right after sliding showed lower resistance for positive electric current conditions. After detaching and rejoining the samples onto the same surface and fresh surface respectively, the resistance dropped as expected. The combination of High W-DLC – High W-DLC contact showed by far the best conductivity as well as friction properties.

Surface Analysis

Wear scars on the surface of both counterparts were analyzed using an optical microscope. The wear track profiles presented in Figure 36 correspond to the width and depth of the wear scar. High W-DLC – High W-DLC contact displayed excellent low wear properties. Wear was almost non existent for no current and positive electric current conditions, while some wear can be observed when negative electric current was applied, which is in agreement with higher resistance observed in voltage drop measurements for negative currents. Black spots, that can be seen in Figure 37 on the ball sample's worn surface, could be related to electric current flow scars during static voltage drop measurements.

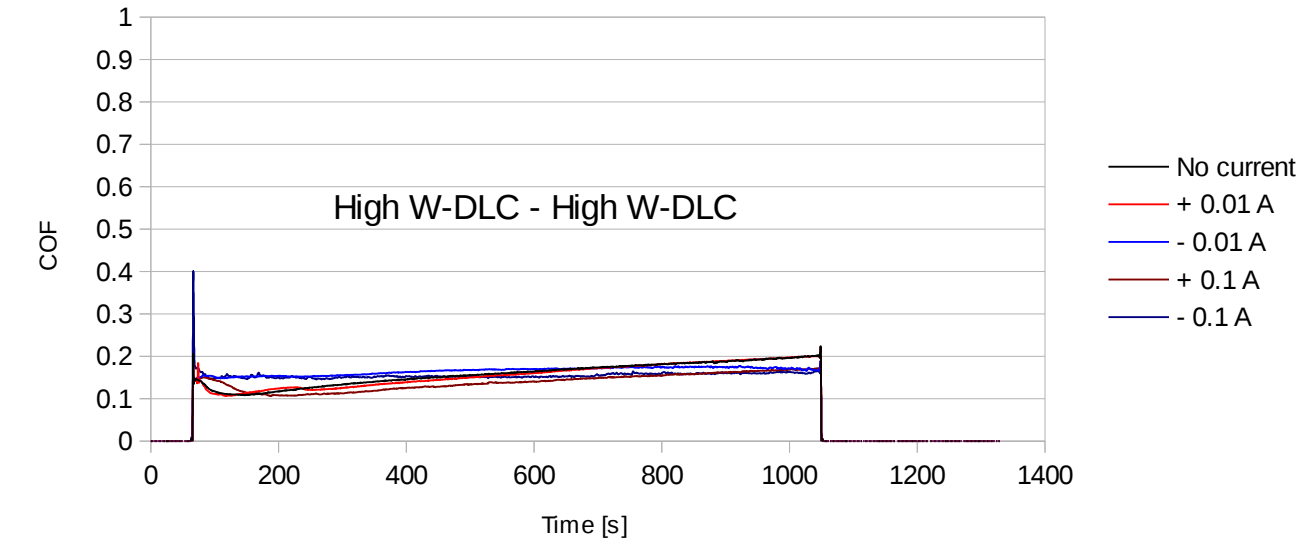

(a)

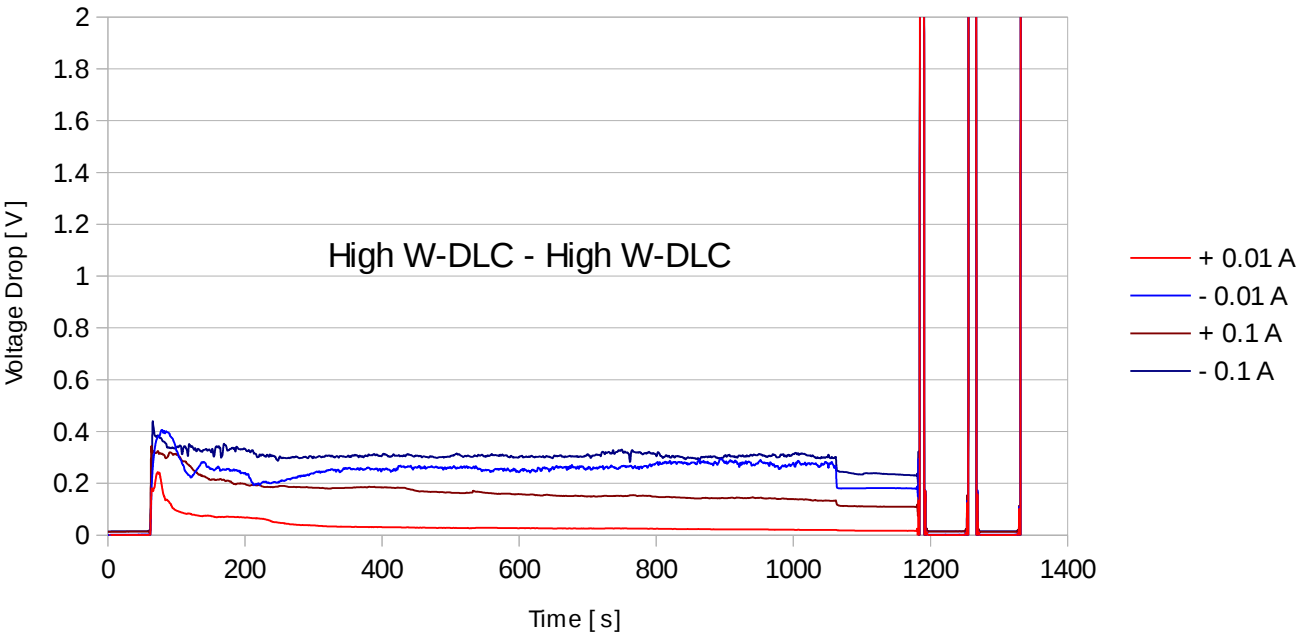

(b)

Figure 35: Coefficient of friction (a) and Voltage drop (b) of High W-DLC – High W-DLC contact

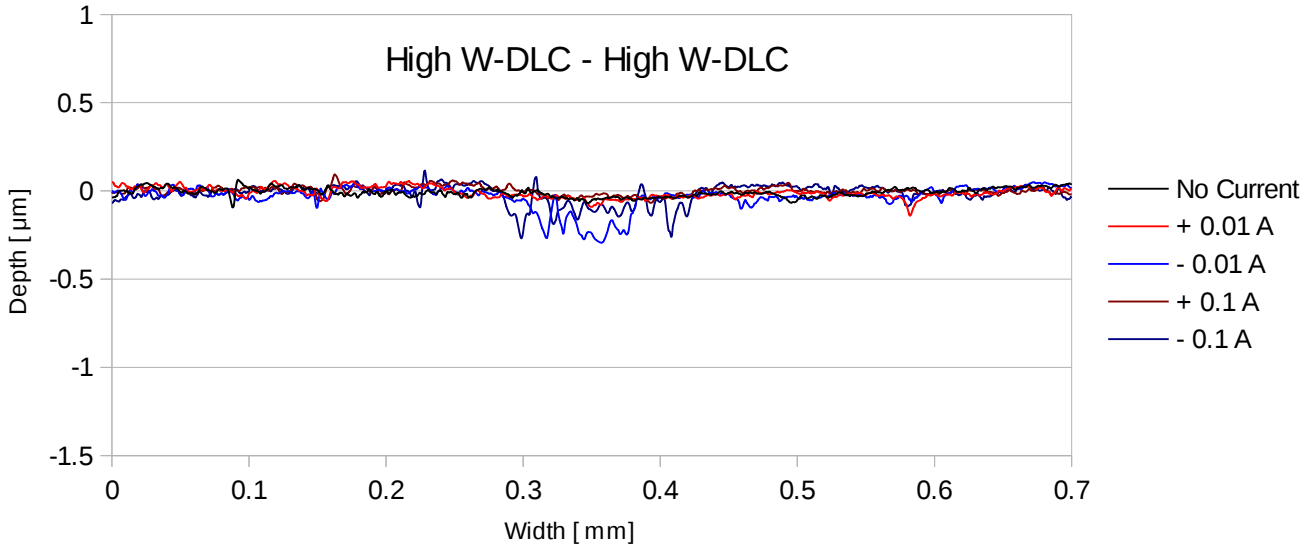

Figure 36: Wear scar profiles of High W-DLC – High W-DLC contact

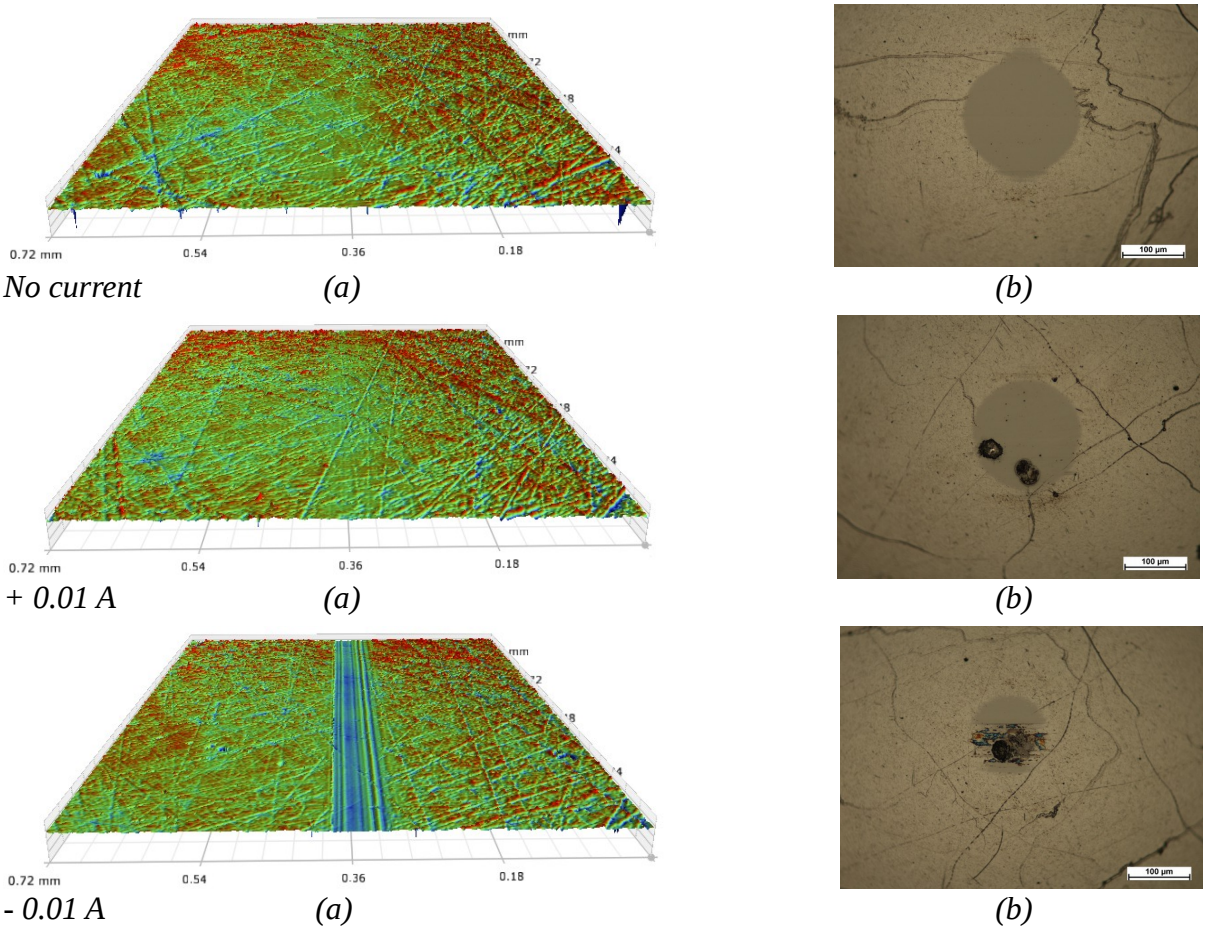

No current *(a)* *(b)*

+ 0.01 A *(a)* *(b)*

- 0.01 A *(a)* *(b)*

Figure 37: Analysis of High W-DLC disc and High W-DLC ball wear scars obtained under different current conditions using 3D microscope (a) to analyze disc wear scars and optical microscope (b) for the observation of the ball surface counterpart

4.6 Summary of Results

Average friction coefficients and voltage drops for all material combinations are presented in Figure 38. It can instantly be seen that Steel – Steel contact has substantially higher coefficient of friction compared to all other material pairs. Comparing only DLC coating material combinations, it can also be observed that in general DLC coatings paired together exhibited lower coefficient of friction than DLC – Steel material combinations. This confirms DLC coatings excellent tribological properties in dry sliding conditions. Material pairs mainly exhibited similar average friction coefficients across all current conditions for a given material combination. Variation of COF was observed only for certain material pairs and electric current conditions. Low Ti-DLC coating coupled together and High Ti-DLC paired with steel exhibited an increased COF when positive electric current of 0.1 A was applied. Steel – Steel and High Ti-DLC – High Ti-DLC contacts showed lower COF when negative current was applied, which was even lower than when there was no current present. Negative current conditions had a reverse effect on the COF of Low W-DLC – Steel contact, where higher COF was observed for negative currents. High W-DLC in both material combinations exhibited lower friction coefficients for higher currents of 0.1 A. The COF for currents of 0.1 A was even lower than when no current was applied. On average, the best friction coefficients were observed for DLC – DLC contact, follower by DLC – Steel and the far worst being Steel – Steel contacts.

Electrical resistance measurements showed a large difference between static resistance of the contact and the resistance of the contact during sliding. During static resistance measuring, the resistance was low, showing a voltage drop around 0.001 V, independent of electric current conditions. During sliding, the resistance of the contact increased substantially for all current conditions. This goes to show that the resistance of the sliding contact is not only dependent on the resistance of the paired materials but also on the environmental parameters, that effect the cumulative resistance. Electrical resistance average comparison revealed how greatly resistance varied between different material combinations and different electric current conditions during sliding. There are some trends that can still be observed for certain material combinations an electric current conditions. Steel – Steel contact exhibited lower resistance than most of DLC coating material combinations, except for when negative current of 0.1 A was applied. The unusual resistance could be attributed to the unpredictable formation of the highly resistive oxide layer on the steel surface. In general, the resistance was the lowest for DLC – DLC contact pairs with higher dopant concentrations. This trend can ideally be observed for measurements under negative electric current. For both 0.01 A and 0.1 A negative current, the resistance drops accordingly with increased doping element concentration and DLC – DLC contact combination for all DLC coating material pairs. The same trend can be observed for all W-DLC coating measurements. Positive currents showed greater resistance in the majority of measurements except for High W-DLC – High W-DLC contact, which displayed the lowest measured voltage drops all-round for both positive currents. Overall, the lowest resistance was observed for High W-DLC – High W-DLC material combination.

Material combination with the lowest average COF, lowest resistance, lowest wear rate and subsequently the most promising material pair is High W-DLC – High W-DLC, followed by High Ti-DLC – High Ti-DLC, Low Ti-DLC – Low Ti-DLC, High Ti-DLC – Steel, High W-DLC – Steel, Low W-DLC – Steel, Low Ti-DLC – Steel and Steel – Steel. Steel – Steel contact exhibited relatively good electric conductivity properties but due to its high COF and wear rates in dry sliding conditions, it was chosen as the least favorable material combination for electrical contact applications.

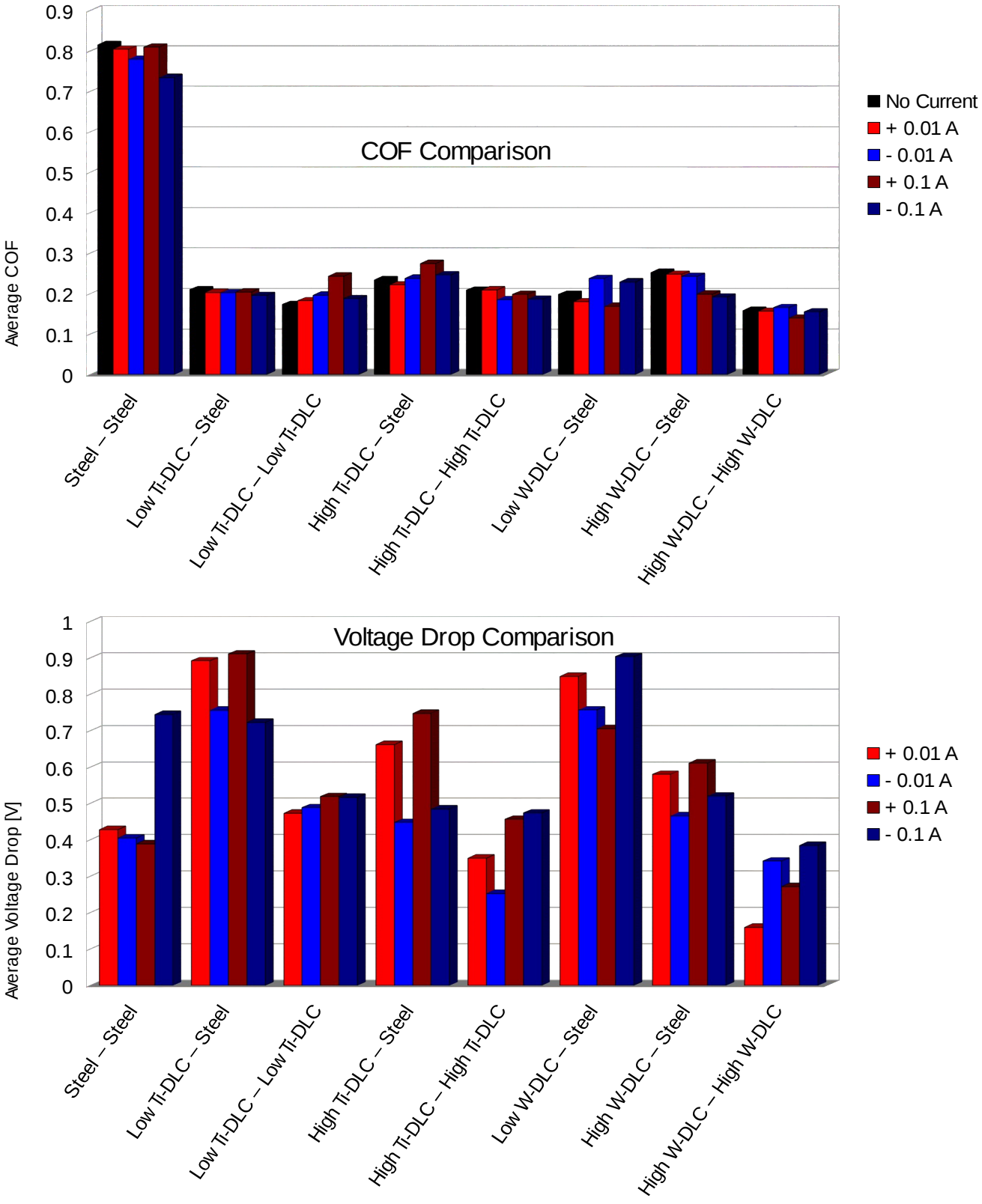

Figure 38: Comparison of average COF and Voltage drop for all material combinations

5. Conclusions and Future Work

Four different coatings – Low Ti-DLC, High Ti-DLC, Low W-DLC and High W-DLC – and steel were analyzed under dry reciprocating sliding and various electric current (DC) conditions. The following conclusions could be drawn from the present study:

1. All material combinations conducted direct current when in sliding contact, therefore all selected coatings were conductive. The conductivity varied between material combinations. The most favorable conductivity properties were observed for High W-DLC – High W-DLC contact. This combination also presented the lowest friction and wear properties, making it the best material combination tested. The most adverse combinations of materials among DLC coatings were Low Ti-DLC – Steel and Low W-DLC – Steel, where relatively high resistance was observed coupled with unstable friction and higher wear rates. For Steel – Steel contact, relatively high conductivity was observed but due to high friction coefficient and high wear rate, did not show promise for electrical applications.
2. Doped elements in DLC and the amount of doping elements had a great effect on the electrical properties of the coating. Increased doping concentrations lead to higher electric conductivity of the coatings in contact for both doping elements used in this work.
3. There was a considerable distinctions between static resistance and sliding resistance of the contact. Sliding increased the resistance of the contact substantially due to the conductivity conditions present in the contact. The tribological properties of the contact therefore play an important part in the collective resistance of the contact.
4. Electric resistance of the coatings was affected by the changes of the coefficient of friction. When there was a spike in the COF, an analogous drop in resistance could be observed and when there was a drop in friction, resistance in the contact increased. Higher coefficient of friction could be attributed to some adhesion being present in the contact. The cold welding of the asperities could cause a drop in resistance but also promote high COF. Electric resistance was inversely proportional to the COF. However, the correlation between COF and resistance could only be made for the same material combination.
5. Electric current did not explicitly affect the coefficient of friction of the materials in contact, but it might have had some indirect influence on the friction by promoting higher wear of surfaces in contact and therefore incidentally causing a rise in friction. Substantial wear in the form of tearing of the coating, caused by high electric current density could be observed for the following material combinations: Low Ti-DLC – Low Ti-DLC, Low W-DLC – Steel.
6. Direction of electric current flow had a noticeable influence on resistance of the contact and wear rate. This could easily be seen for High Ti-DLC – Steel, Low Ti-DLC – Steel and Low Ti-DLC – Low Ti-DLC contacts where positive currents exhibited higher resistance and larger wear scars. It could also be noted that the resistance was lower at negative electric current conditions for all DLC – Steel contacts except for Low W-DLC – Steel at - 0.1 A.
7. Voltage drop measurements of material combinations showed similar voltage drop measurements, regardless of the amount of current applied in the contact, which differed by a factor of ten (0.01 A and 0.1 A). By voltage drop measurements obtained and following Ohm's law, it could be concluded that at higher current densities, the resistance of the contact had dropped.

8. Material combinations where DLC coatings were coupled together exhibited steadier coefficient of friction and resistance with less spikes and scattering. This could be attributed to the excellent tribological properties of DLC coatings in dry sliding conditions, which enabled steady sliding with low COF and stable electric conductivity, making them more appropriate for electrical applications, where stable electric conductivity is desired.

Future studies could focus on a separate study of interlayers and coatings and how each component contributes to the overall resistance of the whole coating. The study of coatings electrical properties in sliding contact with addition of different oils could also be the subject of future research in order to determine if lubricated contacts could be used in electrical applications for improved tribological performance. Further research of DLC coatings in electric contact applications should also compare DLC coatings electric and tribological properties to graphite/copper material combinations, which are widely used in electrical applications. This would give a better estimation of the DLC coatings potential for replacing graphite/copper materials in electrical contacts.

6. References

[1] A. Grill. Diamond-like carbon: state of the art, *Diamond and Related Materials, 8 (1999),* 428–434

[2] R.S. Li, E.Q. Xie, M. Zhou, Z.X. Zhang, T. Wang, B.A. Lu, E.Q. Xie. Effect of deposition voltage on the field emission properties of electrodeposited diamond-like carbon films, *Applied Surface Science, 255 (2009),* 4754–4757

[3] Y. Lifshitz. Diamond-like carbon- Present status, *Diamond and Related Materials, 8 (1999),* 1659–1676

[4] D. Bootkul, B. Supsermpol, N. Saenphinit, C. Aramwit, S. Intarasiri. Nitrogen doping for adhesion improvement of DLC film deposited on Si substrate by Filtered Cathodic Vacuum Arc (FCVA) technique, *Applied Surface Science, 310 (2014),* 284–292

[5] Š. Meškinis, V. Kopustinskas, A. Tamulevičien, S. Tamulevičius, G. Niaura, J. Jankauskas, R. Gudaitis. Ion beam energy effects on structure and properties of diamond like carbon films deposited by closed drift ion source, *Vacuum, 84 (2010),* 1133–1137

[6] L. Quang, B. Zhang, Y. Zhou, J. Zhang. Improving the internal stress and wear resistance of DLC films by low content Ti doping, Solid State Science, 20 (2013), 17–22

[7] M. Guerino, M. Massi, H.S. Maciel, C. Otani, R.D. Mansano. The effects of the nitrogen on the electrical and structural properties of the diamond-like carbon (DLC) films, *Microelectronics Journal, 34 (2003),* 639–641

[8] A. Matthews, S.S. Eskildsen. Engineering applications for diamond-like carbon, *Diamond and Related Materials, 3 (1994),* 902–911

[9] J. Vetter. 60 years of DLC coatings: Historical highlights and technical review of cathodic arc processes to synthesize various DLC types, and their evolution for industrial applications. *Surface & Coatings Technology (2014)*

[10] C. Donnet, A. Erdemir. Diamon-like Carbon Films: A Historical Overview, Tribology of Diamond-Like Carbon Films: Fundamentals and Applications. *Springer Science* (2008)

[11] J. Robertson. Diamond-like amorphous carbon, *Materials Science and Engineering, R 37 (2002),* 129–281

[12] I. Yasar, A. Canakci, F. Arslan. The effect of brush spring pressure on the wear behavior of copper–graphite brushes with electrical current, Tribology International, 40 (2007), 1381–1386

[13] M.P. Siegal, T.A. Friedmann, J.P. Sullivan, J. Mikkalson, F. Dominguez, S.R. Kurtz, D.R. Tallant, R.L. Simpson, K.F. McCarty, L Bemardez, D. Dibble, P.B. Mirkarimi. Diamond and Diamond-Like Carbon Films for Advanced Electronic Applications, *SAND, 96–0516 (1996)*

[14] Generators and Dynamos. Available: http://www.edisontechcenter.org/generators.html. Last accessed 15th June 2015

[15] J. Robertson. Classification of Diamond-like Carbons, Tribology of Diamond-Like Carbon Films: Fundamentals and Applications. *Springer Science* (2008)

[16] S. Wan, L. Wang, Q. Xue. An electrochemical strategy to incorporate iron into diamond like carbon films with magnetic properties, *Electrochemistry Communications, 11 (2009),* 99–102

[17] G. Ma, S. Gong, G. Lin, L. Zhang, G. Sun. A study of structure and properties of Ti-doped DLC film by reactive magnetron sputtering with ion implantation, *Applied Surface Science, 258 (2012)*, 3045–3050

[18] T. Nakahigashi, Y. Tanaka, K. Miyake, H. Oohara. Properties of flexible DLC film deposited by amplitude-modulated RF P-CVD, *Tribology International, 37 (2004)*, 907–912

[19] J. Robertson. Properties of diamond-like carbon, *Surface and Coatings Technology, 50 (1992)*, 185–203

[20] D. Bootkul, S. Intarasiri, C. Aramwit, U. Tippawan, L.D. Yu. Formation of thin DLC films on SiO2/Si substrate using FCVAD technique, *Nuclear Instruments and Methods in Physics Research, B 307 (2013)*, 147–153

[21] F.M. Kimock, B.J. Knapp. Commercial applications of ion beam deposited diamond-like carbon (DLC) coatings, *Surface and Coatings Technology, 56 (1993)*, 273–279

[22] B. Bhushan. Nanotribology of Ultrathin and Hard Amorphous Carbon Films, Tribology of Diamond-Like Carbon Films: Fundamentals and Applications. *Springer Science* (2008)

[23] Š. Meškinisa, K. Šlapikasa, R. Gudaitisa, S. Tamulevičiusa, V. Kopustinskasa, A. Guobiene, G. Niaurab. SiOx-doped DLC films: Charge transport, dielectric properties and structure, *Vacuum, 82 (2008)*, 617–622

[24] S. Wan, L. Wang, J. Zhang, Q. Xue. Field emission properties of DLC and phosphorus-doped DLC films prepared by electrochemical deposition process, *Applied Surface Science, 255 (2009)*, 3817–3821

[25] J. C. Sánchez-López, A. Fernández. Doping and Alloying Effects on DLC Coatings, Tribology of Diamond-Like Carbon Films: Fundamentals and Applications. *Springer Science* (2008)

[26] N.K. Manninen, F. Ribeiro, A. Escudeiro, T. Polcar, S. Carvalho, A. Cavaleiro. Influence of Ag content on mechanical and tribological behavior of DLC coatings. *Surface & Coatings Technology, 232* (2013), 440–446

[27] A.P. Mousinho, R.D. Mansano. Influence of the plasma parameters and nitrogen addition on the electrical characteristics of DLC films deposited by inductively coupled plasma deposition, *Applied Surface Science, 254 (2007)*, 189–192

[28] Xingbin Yan, Tao Xu, Gang Chen, Shengrong Yang*, Huiwen Liu. Study of structure, tribological properties and growth mechanism of DLC and nitrogen-doped DLC films deposited by electrochemical technique, *Applied Surface Science, 236 (2004)*, 328–335

[29] I. Kleps, D. Nicolaescu, I. Stamatin, A. Correia, A. Gil, A. Zlatkin. Field emission properties of silicon carbide and diamond-like carbon (DLC) films made by chemical vapour deposition techniques, *Applied Surface Science, 146 (1999),* 152–157

[30] H.S. Zhang, J.L. Endrino, A. Anders. Comparative surface and nano-tribological characteristics of nanocomposite diamond-like carbon thin films doped by silver, *Applied Surface Science, 255 (2008)*, 2551–2556

[31] X. Shia, L. Guo, Y. Bai, L. Qiao. Characterization of coating probe with Ti-DLC for electrical scanning probe microscope, *Applied Surface Science, 257 (2011)*, 7238–7244

[32] M. Guerino, M. Massi, H.S. Maciel, C. Otani, R.D. Mansano, P. Verdonck, J. Libardi. The influence of nitrogen on the dielectric constant and surface hardness in diamond-like carbon (DLC) films, *Diamond and Related Materials, 13 (2004)*, 316–319

[33] A. Tamulevičiene, V. Kopustinskas, G. Niaura, Š. Meškinis, S. Tamulevičius. Multiwavelength Raman analysis of SiOx and N containing amorphous diamond like carbon films, *Thin Solid Films (2014)*

[34] A. Grill. Electrical and optical properties of diamond-like carbon. *Thin Solid Films, 355-356* (1999), 189–193

[35] E. Staryga, G.W. Bak. Relation between structure and electrical properties of diamond-like carbon thin films, Diamond & Related Materials, 14 (2005), 23–24

[36] A. Grill, V. Patel, S. Cohen. Electrical resistivities of diamond-like carbon, *Diamond and Related Materials, 3 (1994)*, 281–284

[37] Š. Meškinis, R. Gudaitis, V. Kopustinskas, S. Tamulevičius, K. Šlapikas. Piezoresistive, optical and electrical properties of diamond like carbon and carbon nitride films, *Diamond & Related Materials, 19 (2010)*, 1249–1253

[38] K. Honglertkongsakul, P.W. May, B. Paosawatyanyong. Electrical and optical properties of diamond-like carbon films deposited by pulsed laser ablation. *Diamond & Related Materials, 19 (2010)*, 999–1002

[39] Š. Meškinis, R. Gudaitis, V. Kopustinskas, S. Tamulevičius. Electrical and piezoresistive properties of ion beam deposited DLC films. *Applied Surface Science, 254* (2008), 5252–5256

[40] S. Miyagawa, S. Nakao, J. Choi, M. Ikeyama, Y. Miyagawa. Electrically conductive diamond-like carbon coatings prepared by plasma-based ion implantation with bipolar pulses, *New Diamond and Frontier Carbon Technology, Vol. 16 (2006)*, No. 1

[41] E. Staryga, G.W. Bak, M. Dłuzniewski. Some electrical properties of diamond-like carbon thin films, Vacuum, 74 (2004), 325–330

[42] K. Nakayama. Triboemission and Triboplasma Generation with DLC Films, Tribology of Diamond-Like Carbon Films: Fundamentals and Applications. *Springer Science* (2008)

[43] J.L. Endrino, D. Horwat, R. Gago, J. Andersson, Y.S. Liu, J. Guo, A. Anders. Electronic structure and conductivity of nanocomposite metal (Au, Ag, Cu, Mo)-containing amorphous carbon films, *Solid State Sciences, 11 (2009)*, 1742–1746

[44] K. Bewilogua, C.V. Cooper, C. Specht, J. Schroder, R. Wittorf, M. Grischke. Effect of target material on deposition and properties of metal-containing DLC Me-DLC coatings, *Surface and Coatings Technology, 127 (2000)*, 224–232

[45] S.J. Dikshit, P. Leel, S.B. Ogale, S.T. Kshiragar. Influence of in-process copper incorporation on the quality of diamond-like carbon films deposited by pulsed laser deposition technique, J. Mater. Res, 11 (1996), 2236–2241

[46] Y. Suzuki, M. Watanabe, T. Toda, T. Fujii. Development of electrically conductive DLC coated stainless steel separators for polymer electrolyte membrane fuel cell, *Journal of Physics: Conference Series, 441 (2013)*

[47] S. Reuter, B. Weßkamp, R. Buscher, A. Fischer, B. Barden, F. Loer, V. Buck. Correlation of structural properties of commercial DLC-coatings to their tribological performance in biomedical applications, *Wear, 261 (2006)*, 419–425

[48] M. Sedlaček, B. Podgornik, J. Vižintin. Tribological properties of DLC coatings and comparison with test results: Development of a database, Materials Characterization, 59 (2008), 151–161

[49] K. Simonović, F. Marinković, D. Dudić, M. Kalin. Surface Dielectric Properties of Different Diamond-like Carbon (DLC) Coatings

[50] Ball on Flat Sliding War Test Using Micro-Tribometer mod. CETR-UMT2. Available: http://www.cetr.com/eng/services/pdf/ASTM%20G133-95%20reciprocating%20ball%20on%20flat.pdf. Last accessed 15th June 2015

Appendix

Wear Scar Images

Steel – Steel

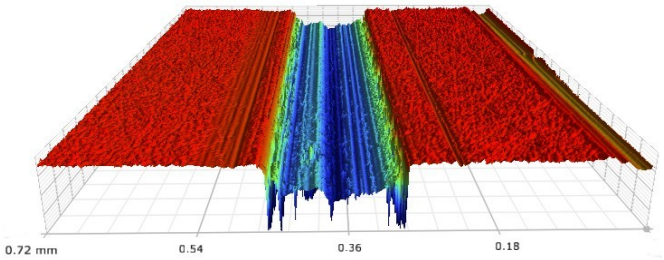

+ 0.1 A *(a)* *(b)*

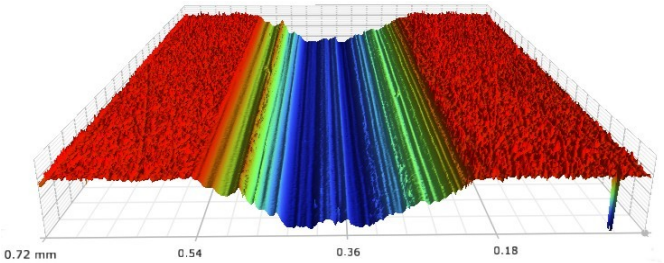

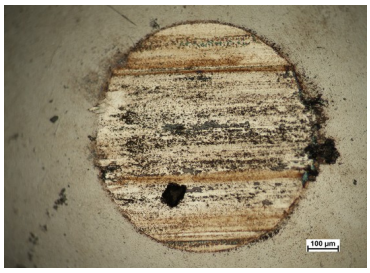

- 0.1 A *(a)* *(b)*

Figure 39: Analysis of Steel disc and Steel ball wear scars obtained under + 0.1 A and – 0.1 A current conditions using 3D microscope (a) to analyze disc wear scars and optical microscope (b) for the observation of the ball surface counterpart

Low Ti-DLC – Steel

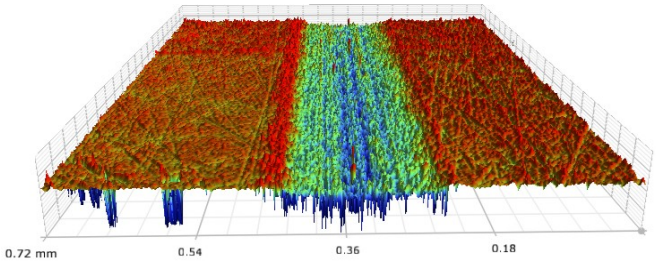

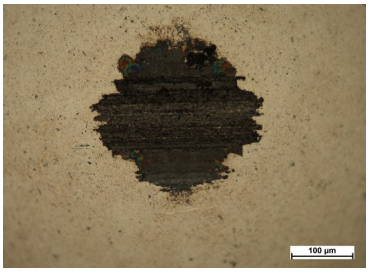

+ 0.1 A *(a)* *(b)*

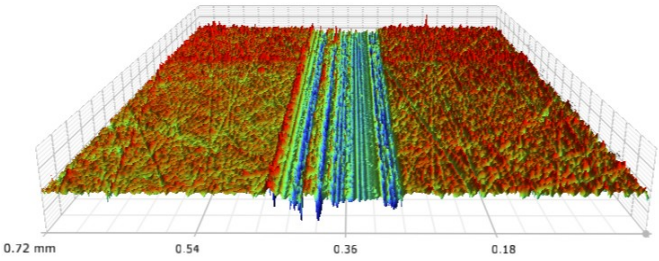

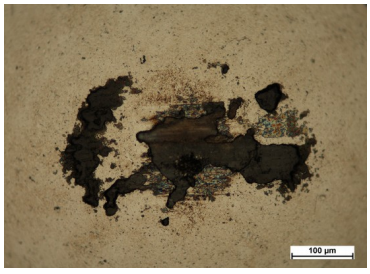

- 0.1 A *(a)* *(b)*

Figure 40: Analysis of Low Ti-DLC disc and Steel ball wear scars obtained under + 0.1 A and – 0.1 A current conditions using 3D microscope (a) to analyze disc wear scars and optical microscope (b) for the observation of the ball surface counterpart

Low Ti-DLC – Low Ti-DLC

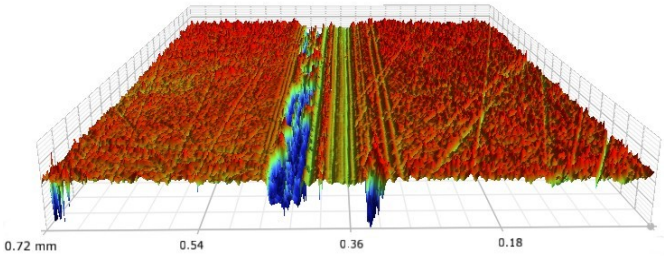

+ 0.1 A *(a)*

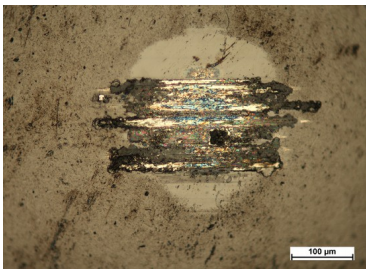

(b)

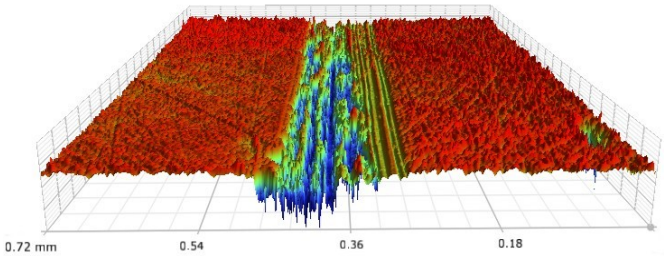

- 0.1 A *(a)*

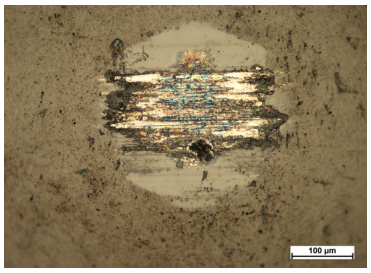

(b)

Figure 41: Analysis of Low Ti-DLC disc and Low Ti-DLC ball wear scars obtained under + 0.1 A and – 0.1 A current conditions using 3D microscope (a) to analyze disc wear scars and optical microscope (b) for the observation of the ball surface counterpart

High Ti-DLC – Steel

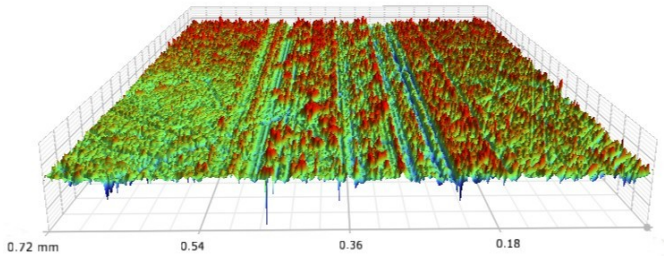

+ 0.1 A *(a)*

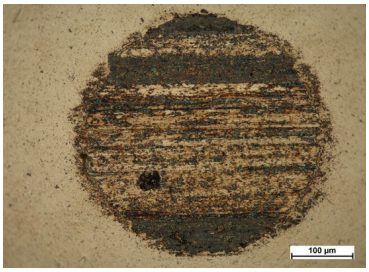

(b)

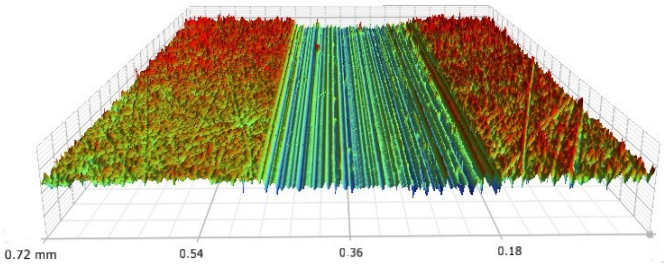

- 0.1 A *(a)*

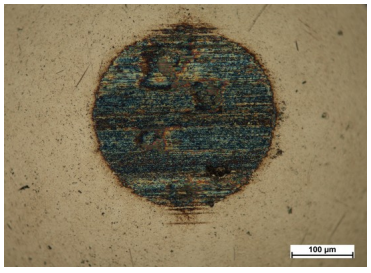

(b)

Figure 42: Analysis of High Ti-DLC disc and Steel ball wear scars obtained under + 0.1 A and – 0.1 A current conditions using 3D microscope (a) to analyze disc wear scars and optical microscope (b) for the observation of the ball surface counterpart

High Ti-DLC – High Ti-DLC

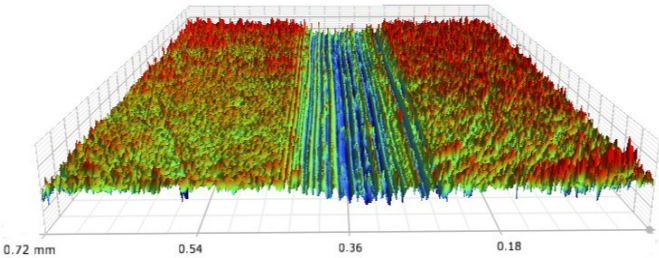

+ 0.1 A *(a)*

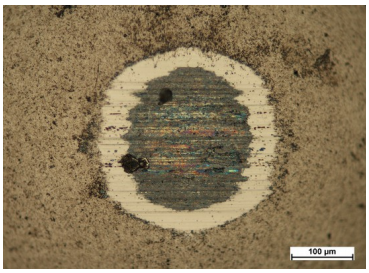

(b)

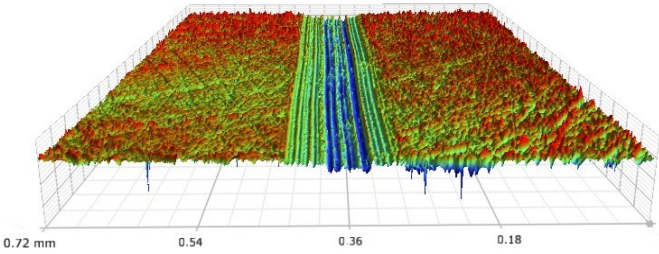

- 0.1 A *(a)*

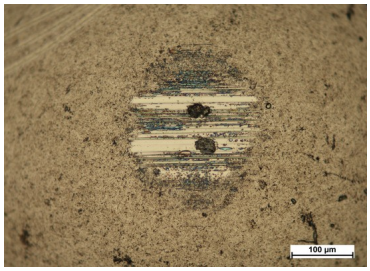

(b)

Figure 43: Analysis of High Ti-DLC disc and High Ti-DLC ball wear scars obtained under + 0.1 A and – 0.1 A current conditions using 3D microscope (a) to analyze disc wear scars and optical microscope (b) for the observation of the ball surface counterpart

Low W-DLC – Steel

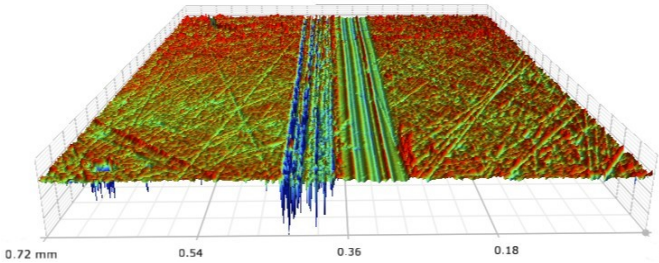

+ 0.1 A *(a)*

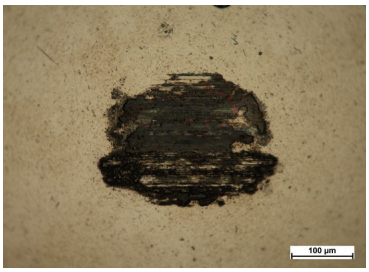

(b)

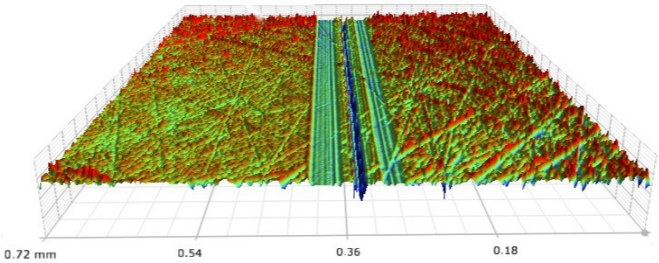

- 0.1 A *(a)*

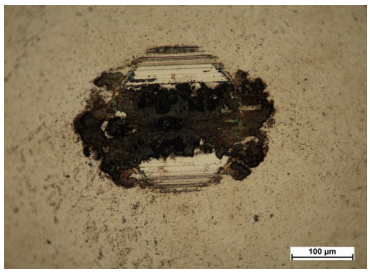

(b)

Figure 44: Analysis of Low W-DLC disc and Steel ball wear scars obtained under + 0.1 A and – 0.1 A current conditions using 3D microscope (a) to analyze disc wear scars and optical microscope (b) for the observation of the ball surface counterpart

High W-DLC – Steel

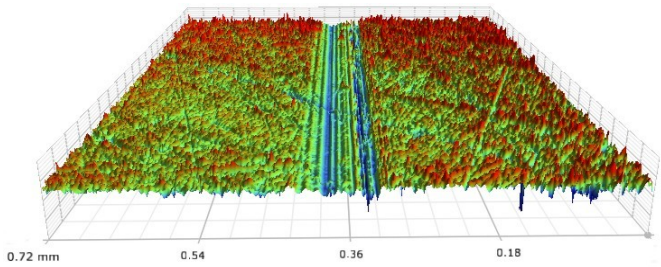

+ 0.1 A *(a)*

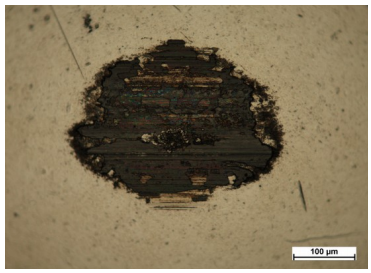

(b)

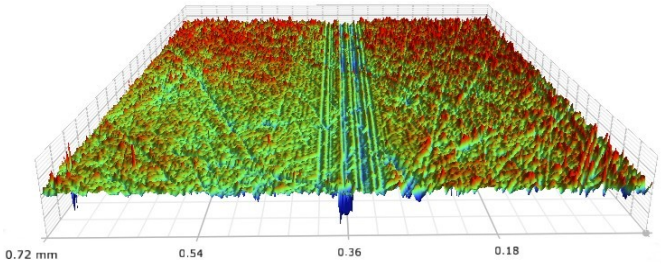

- 0.1 A *(a)*

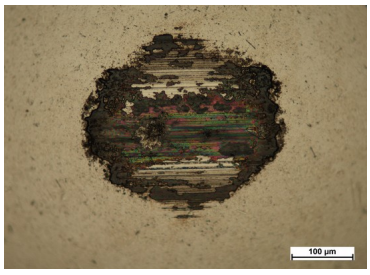

(b)

Figure 45: Analysis of High W-DLC disc and Steel ball wear scars obtained under + 0.1 A and – 0.1 A current conditions using 3D microscope (a) to analyze disc wear scars and optical microscope (b) for the observation of the ball surface counterpart

High W-DLC – High W-DLC

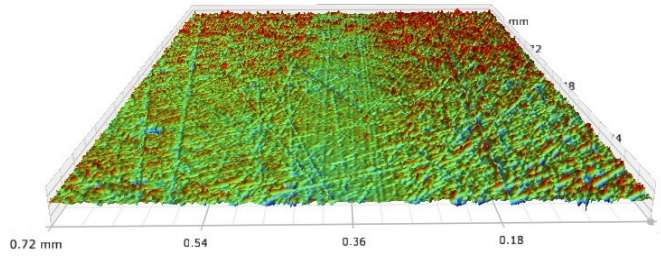

+ 0.1 A *(a)*

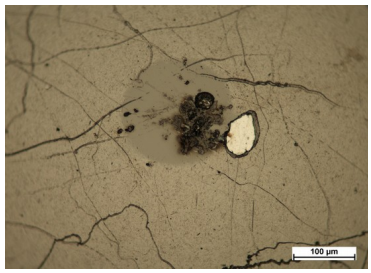

(b)

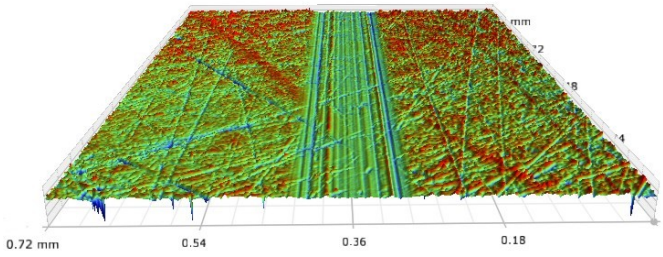

- 0.1 A *(a)*

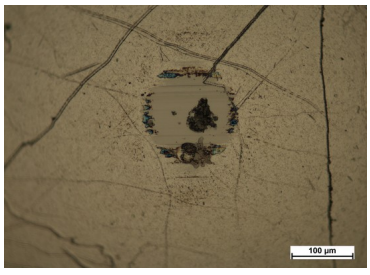

(b)

Figure 46: Analysis of High W-DLC disc and High W-DLC ball wear scars obtained under + 0.1 A and – 0.1 A current conditions using 3D microscope (a) to analyze disc wear scars and optical microscope (b) for the observation of the ball surface counterpart